

University of Alberta

**A Preliminary Study on Pyrolysis and Gasification of
Asphaltenes and Coal-Asphaltenes Slurry in Entrained Flow
Reactor**

by

Behnam Berahman

A thesis submitted to the Faculty of Graduate Studies and Research
in partial fulfillment of the requirements for the degree of

Master of Science

in

Chemical Engineering

Department of Chemical and Materials Engineering

©Behnam Berahman

Fall 2012

Edmonton, Alberta

Permission is hereby granted to the University of Alberta Libraries to reproduce single copies of this thesis and to lend or sell such copies for private, scholarly or scientific research purposes only. Where the thesis is converted to, or otherwise made available in digital form, the University of Alberta will advise potential users of the thesis of these terms.

The author reserves all other publication and other rights in association with the copyright in the thesis and, except as herein before provided, neither the thesis nor any substantial portion thereof may be printed or otherwise reproduced in any material form whatsoever without the author's prior written permission.

ABSTRACT

The aim of this work is to study pyrolysis of coal-asphaltenes slurry in an atmospheric entrained flow reactor. Athabasca asphaltenes and Genesee coal, both from Alberta in Canada, were selected as the feedstock. Char characteristics and the structure of asphaltenes and slurry chars including morphology, particle size distribution and surface area were determined. Besides, the reactivity of chars obtained from the fast pyrolysis was measured and the effect of temperature, heating rate and residence time on the produced char reactivity was investigated. Furthermore, the gasification kinetics of the asphaltenes and slurry chars with O_2 were studied and a reaction kinetic was proposed based on the TGA results. The results revealed that in the slurry char, asphaltenes part and coal part involve in the reaction with oxygen separately. It is also concluded that the reactivity of the chars obtained from the slurry of coal-asphaltenes was lower than the asphaltenes chars.

ACKNOWLEDGEMENTS

I would like to express my gratitude to my supervisor, Dr. Rajender Gupta, for his guidance, patience and support for doing this research project.

I gratefully thank Dr. Frank Vejahati for his valuable support on the course of this project. I am grateful in every possible way and hope to keep up our collaboration in the future.

I thank Dr. Vinay Prasad and Dr. Shayan Karimipour for their advice and comments.

I also would like to appreciate the help of all the technicians and staff at Chemical and Materials Department of University of Alberta for providing laboratory resources and services.

I thank the Canadian Centre for Clean Coal/Carbon and Mineral Processing Technologies (C5MPT) and Helmholtz Alberta Initiative (HAI) for the funding of this project.

Table of Contents

CHAPTER 1 Introduction.....	1
1.1 Feedstock	1
1.2 Gasification	2
1.2.1 Gasification technologies.....	5
1.3 Slurry gasification	7
1.4 How this thesis is organized	9
1.5 Objectives	11
CHAPTER 2 Literature Review	12
2.1 Asphaltenes	12
2.2 Rheology of asphaltenes and slurries	15
2.2.1 Asphaltenes viscosity.....	15
2.2.2 Viscosity of slurries.....	16
2.3 Slurry atomization	17
2.3.1 Principles of atomization.....	17
2.3.2 Primary Breakup.....	18
2.3.3 Secondary Breakup.....	20
2.3.4 Droplet size distribution.....	21
2.3.5 Types of sprays.....	23
2.4 Pyrolysis and gasification of slurries.....	25

2.4.1	Coal-water slurry gasification	25
2.4.2	Bio-oil and biomass slurry pyrolysis and gasification.....	27
2.5	Asphaltenes and heavy oil pyrolysis and gasification	30
2.5.1	Asphaltenes char characteristics	33
2.6	Kinetics of asphaltenes gasification.....	35
2.6.1	Analysis of the mass transfer effect	35
2.6.2	Effect of heating rate	39
2.6.3	Effect of partial pressure	42
CHAPTER 3	Pyrolysis Experiments	45
3.1	Experimental setup	45
3.2	Fuel characterization.....	49
3.3	Char preparation.....	50
3.4	Asphaltenes char characteristics	51
3.4.1	Char Reactivity.....	53
3.4.2	Morphological analysis of asphaltenes chars.....	56
3.4.3	Particle size distribution.....	60
3.5	Characteristics of slurry chars	61
3.5.1	Proximate and ultimate analyses.....	61
3.5.2	Morphology analysis of slurry chars	63
3.5.3	Reactivity of slurry chars.....	65
3.5.4	Particle size distribution.....	70

3.6	Chapter findings and conclusion.....	72
CHAPTER 4 Kinetics of the reactions of asphaltenes and slurry chars		
	with O₂.....	74
4.1	The feedstock.....	74
4.2	Char preparation.....	75
4.3	TGA experiments.....	75
4.4	Treatment of TGA results.....	77
4.4.1	Slurry char-O ₂ reaction.....	78
4.4.2	Asphaltenes char-O ₂ reaction.....	84
4.5	Chapter findings and conclusion.....	85
CHAPTER 5 Conclusions and Recommendations87		
5.1	Conclusions.....	87
5.2	Recommendations for future work.....	89
6	References.....	90

List of Tables

Table 2-1 Typical properties of asphaltenes from various origins	14
Table 3-1 - Proximate and ultimate analyses of asphaltenes	49
Table 3-2 - Proximate and ultimate analysis of asphaltenes chars	52
Table 3-3 - Proximate and ultimate analysis of slurry chars	62
Table 4-1 - Summary of results for kinetic of char-O ₂ reaction	86

List of Figures

Figure 1-1 Temperature profile for (a) dry fed entrained flow gasifier and (b) slurry fed entrained flow gasifier	8
Figure 2-1 - “Long diagram” showing high polarity, aromaticity and molecular weight of asphaltenes.....	13
Figure 2-2 - Viscosity of asphaltenes from Canadian bitumen	15
Figure 2-3 Effect of the solid loading on the shear rate to viscosity profile in coal-water slurries (particle size of 250-500 μm)	16
Figure 2-4 - Droplet formation steps	18
Figure 2-5 - Primary breakup regimes	20
Figure 2-6 - Secondary breakup regimes	21
Figure 2-7 - Schematic of a particle size analyzer.....	22
Figure 2-8-Schematic of an effervescent atomizer	23
Figure 2-9 – Coal-water slurry viscosity vs. coal concentration	26
Figure 2-10 - Syngas composition from bio-oil gasification at different temperatures	29
Figure 2-11 - Dealkylation of side aliphatic chains	31
Figure 2-12 - Char samples from Orimulsion extra heavy oil	34
Figure 2-13 - SEM images of the char from asphaltite.....	34
Figure 2-14 - Concentration profile for the reactant gas close to a char particle.....	35
Figure 2-15 - Reactant gas profiles external and internal to a porous char particle.....	37

Figure 3-1 – Schematic diagram of the drop tube and the feeding system.....	47
Figure 3-2 - Cold spray experiments with olive oil/coal slurry	48
Figure 3-3 - Viscosity of the asphaltenes feedstock.....	50
Figure 3-4 - Proximate analysis for asphaltenes chars	52
Figure 3-5 – Asphaltenes chars reactivities with air at 475°C.....	54
Figure 3-6- Effect of pyrolysis residence time on asphaltenes chars reactivity (with air at 475°C)	55
Figure 3-7 - SEM images of chars from asphaltenes at (a) 800°C (b) 1000°C (c) 1100°C and (d) 1400°C	57
Figure 3-8 - Asphaltenes chars at (a) 800°C, (b) 1000°C and (c) 1100°C.....	58
Figure 3-9 - Asphaltenes char particles obtained at 1400°C.....	59
Figure 3-10 - HR-SEM micrographs from waste wood firing. Larger particles covered with ultrafine particles observed by Latva <i>et al.</i> (26).....	59
Figure 3-11 - Particle size distribution for Asphaltenes chars obtained at (a) 1100 °C (b) 1200 °C (c) 1400 °C.....	60
Figure 3-12 - Particle size distribution for asphaltenes chars	61
Figure 3-13 - Proimate analysis of slurry chars.....	63
Figure 3-14 - SEM images of chars from coal-asphaltenes slurry at (a) 1200°C (b) 1300°C and (c) 1400°C with the same residence time of 4 seconds.....	64
Figure 3-15 - Slurry chars obtained at 1400 °C	65
Figure 3-16 - Typical slurry char TGA curve for reaction with O ₂	66
Figure 3-16 - Reactivity of slurry chars with air at 475°C.....	67

Figure 3-17 - TGA curves for slurry and non-slurry chars at (a) 5 sec and (b) 7.5 sec residence time	69
Figure 3-18 - Particle size distribution for slurry chars obtained at (a) 1200 °C (b) 1300 °C (c) 1400 °C	71
Figure 3-19 - Particle size distribution of slurry chars at different pyrolysis temperatures	72
Figure 4-1 - TA instrument Q600 configuration (From TA website)	76
Figure 4-2 - Arhenius plots for reaction of slurry char (obtained at 1300°C) with 1% O ₂ in the range of 425-500°C for (a) Zone I and (b) Zone II	79
Figure 4-3 - Conversion profiles for slurry char (1300 °C) with O ₂ reaction at 475°C and different O ₂ partial pressures.....	80
Figure 4-4 - $\ln(\text{rate})$ vs. $\ln(P_{O_2})$ for reaction of slurry char (obtained at 1300°C) with 0.5, 1 and 2 % at 475°C for (a) Zone I and (b) Zone II	81
Figure 4-5 - Arhenius plots for slurry chars obtained at 1400 °C (a) Zone I and (b) Zone II.....	83
Figure 4-6 - Conversion profiles for asphaltenes chars obtained at 1400°C..	84
Figure 4-7 - Arhenius plot for asphaltenes char obtained at 1400°C.....	85

CHAPTER 1

Introduction

1.1 Feedstock

Asphaltenes and coal are the feedstocks of this work. According to SARA classification, crude oil is classified into four fractions of saturates, aromatics, resins and asphaltenes (1). Asphaltenes are the heaviest part of the crude oil (or bitumen) that are insoluble in n-pentane (or n-heptane) and are soluble in toluene. Canada's raw bitumen production from oil sands has been expected to increase from 1.74 million bpd in 2011 to 5.33 million bpd in 2030, according to Canadian association of petroleum producers (CAPP)

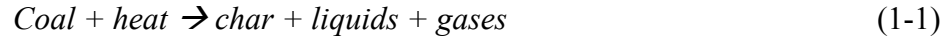
forecast report (2) . Besides, bitumen contains 5-25% asphaltenes, which is the heaviest part of that. On the other hand, asphaltenes are very problematic in bitumen upgrading facilities and they are removed from bitumen in deasphalting units using hydrotreating process. Considering the increasing rate of oil sand production in Alberta, handling asphaltenes would be a real challenge for oil sands industry. Thus, possible potential of using this source for energy production would be absolutely desirable. Moreover, asphaltenes contain high amount of sulfur. Blending asphaltenes with a feedstock containing lower amount of sulfur improves the quality of the feed for gasification. Therefore, the effect of blending coal with asphaltenes in pyrolysis and the characteristics of the chars obtained from pyrolysis as well as the gasification kinetics of chars with oxygen were studied in this work.

1.2 Gasification

Gasification has been used for many years as an integrated part of using problematic fuels for energy generation (3). Gasification is a process that produces a mixture of H₂ and CO gas (i.e. synthesis gas or syngas) theoretically from any carbonaceous fuel. Lower emissions and easier CO₂ capture and emissions control due to the higher temperature and pressure of the exhaust gas are advantages of gasification process, which distinguishes it from other processes such as combustion (3).

Gasification can be summarized into two major steps (3):

- *Pyrolysis* (also called *thermolysis*): during *pyrolysis* organic substances are decomposed into solid residue (i.e. *char*) and volatiles when it is heated up in the absence of oxygen.



- *Gasification*: The reaction between the *char* (from *pyrolysis*) and *gasifying agents* including oxygen, CO₂ or steam:



Moreover, *gasification reactions* can be summarized into these parallel reactions:

Partial oxidation and complete combustion with oxygen are *exothermic reactions* which provide the required heat for the proceeding *gasification reactions* by using much of the oxygen in the *gasifier*.



- *Gasification with CO₂ (Boudouard reaction)*



The reaction is *endothermic* and proceeds very slowly at temperatures below 1000 K and is inhibited by its product.

- *Gasification with steam (water gas reaction)*



This *endothermic reaction* is favoured by elevated temperature and reduced pressure, and in the absence of catalyst, occurs slowly at temperatures below 1200 K.

- *Gasification with hydrogen (hydrogasification reaction)*



Because of some thermodynamic and kinetic limitations hydrogasification reaction is always incomplete and it produces some char residues (3)

The following gas phase reactions are important for the final gas quality to influence H_2/CO ratio. This ratio is important if the gas is for synthesis or hydrogen production.

- *Water-gas shift reaction*



- *Methanation*



Methanation reaction is very slow except at high pressure and increases the caloric value of the gas (3).

The reference conditions for enthalpies of reactions are 298 K and 101.3 kPa.

Since the char that is prepared in the pyrolysis is the main reactant with the gasifying agent, char characteristics including surface area, reactivity and structure have a significant role in gasification and they are very critical in dictating the gasification kinetics. Furthermore, understanding the char gasification kinetics and its reactivity results in better designing of the gasifiers.

1.2.1 Gasification technologies

Gasifiers can be categorized in three major types including fixed (moving) bed, fluidised bed and entrained flow gasifiers.

In the moving bed gasifiers, there is a bed of coal that slowly moves downward. This bed is exposed counter-currently to a stream of oxygen and (or) steam as the temperature moderator. At the top of the gasifier, coals are suddenly heated up by this hot stream that the moisture is abruptly released from the coal. The pyrolysis reaction starts afterwards in a zone called the devolatilization zone, which is more exposed to the hot gases coming up. The gasification zone is located below the devolatilization zone, where char reacts with steam and/or oxygen to produce hydrogen and carbon monoxide. Finally, at the bottom of the gasifier, the residual carbon completely burns with oxygen to generate enough heat for gasification and devolatilization. Moving-bed gasifiers generally consume less oxygen but generate undesired components such as tar, phenol and light hydrocarbons in the pyrolysis phase. Moving-bed gasifiers are normally operated under 3 MPa with a residence time of 0.5-1 hr at higher pressures. Steam is used as moderator in the reactor to keep the temperature below the ash melting point to prevent slagging (3).

In a fluidized bed gasifier, coal is fluidized by an upward stream of oxidant gas. In this case, a good mixing of coal with the gases (i.e. oxidant and moderator) happens which improves the mass and heat transfer within the

reactor. Particle size is usually less than 5mm in a fluidized bed. In addition, there is a limitation for carbon conversion in this type of gasifiers because some particles that are partially consumed by reactions may be entrained by the product gas. Operating temperature is kept below the ash fusion temperature in fluidized beds to avoid the slagging that can cause blockage and interrupt the fluidization. The main advantages of the fluidized bed gasifiers are the feed flexibility and wider range of operating loads (3).

In an entrained flow gasifier with dry feed, pulverised coal co-currently enters the gasifier and mix with air/oxygen and steam as the temperature moderator at the top of the gasifier. Entrained flow gasifiers can operate with all type of coals and feedstock because they operate at very high temperature. Although feed particles (less than 100 μm) remain in the entrained flow only for a few seconds, they rapidly reach the high temperatures of about 1300-1500 $^{\circ}\text{C}$ due to severe heat transfer. Operating at high temperatures allows all carbons in the feed to be converted to product gas representing a complete carbon conversion. In fact, entrained flow gasifiers produce the highest quality syngas with low methane content . Entrained flow gasifiers are used widely for low rank coal gasification and for IGCC applications (3).

1.3 Slurry gasification

There are currently two slurry gasification technologies based on entrained flow gasifiers. The first technology developed by Texaco is a one-stage gasification process and the second one is E-Gas technology that is a two-stage process. The oxidant gas is oxygen in both technologies.

In slurry gasification in an entrained flow gasifier, more time is needed for slurry droplets to reach the slagging temperature at which the minerals in the feed would melt. Therefore, the temperature profile of the feed is different from an entrained flow gasifier with dry feed. Figure 1-1 shows the temperature profile for a slurry entrained flow and a dry feed gasifier. In a single-stage slurry gasifier with coal-water slurry as the feed, water need to be completely converted to steam and then dry feed is raised to the desired operating temperature. This reduces the cold gas efficiency and increases the oxygen consumption of the slurry gasifier compared to a dry feed unit . Also, the high volume of steam needs a larger gasifier which means higher capital cost (3).

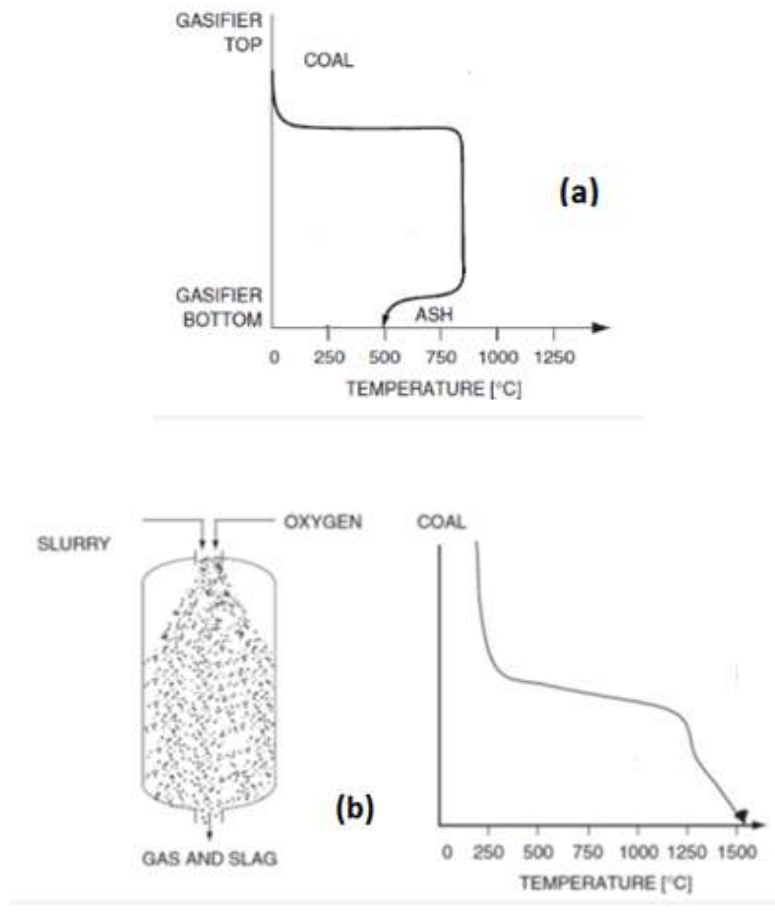


Figure 1-1 Temperature profile for (a) dry fed entrained flow gasifier and (b) slurry fed entrained flow gasifier (Adopted from (3))

Also, in case of coal-water slurry, the water in the feedstock supplies the required steam for gasification and also controls the product gas H_2/CO ratio. Because of the high steam content during the gasification, more CO will be converted to CO_2 by the CO shift reaction resulting in a product gas with higher H_2/CO ratio and higher CO_2 content. This syngas composition is favoured for gasification for the purpose of hydrogen production. Furthermore, the temperature in this system can be controlled by the

oxygen/carbon ratio. Also, it is possible to use other carbonaceous carrier fluids such as bio-oil and heavy oil and asphaltenes. This char will be further gasified and produce more syngas.

The advantages of slurry gasification are listed below (3):

- *Higher maximum practical operating pressure:* The practical maximum pressure in dry-feed gasification is 50 bar while in the slurry feed gasifiers the pressure can reach to about 200 bar.
- *Lower cost of gas compression and carbon capture:* Due to higher operating pressure, there is no compressor needed for gas cleaning. In addition, operating at high pressures reduces the cost of gas compression and carbon capture and storage (CCS) process.
- *Pumping the slurry is less complex* than lock-hoppering and valve systems in dry-feed gasifiers.
- Steam produced in case of water slurries provides *better H_2/CO ratio control and* more CO_2 production during the gasification. After separation of CO_2 from the syngas higher H_2/CO ratio is achieved.

1.4 How this thesis is organized

The second chapter of this thesis is a literature review on the related topics. The chapter is started with properties of asphaltenes. Further, the works on slurry gasification and pyrolysis are reviewed including coal-water

slurries, bio-oil/char and asphaltenes and heavy oil. Moreover, pyrolysis of asphaltenes and its mechanisms are reviewed along with the kinetic studies on asphaltenes gasification. The chapter is continued with the review on rheology of slurries and asphaltenes. Finally, slurry atomization and its principles are mentioned at the end.

The third chapter describes the pyrolysis experiments conducted in this work. After describing the design of the apparatus and feed characterization, it is mentioned in this chapter that how char is prepared from pyrolysis of asphaltenes and slurry feeds. The main part of this chapter is about asphaltenes and slurry char characterization including chars reactivity, morphology and surface area.

The fourth chapter is about the kinetic study of char gasification reactions with O_2 using a thermogravimetric analyzer (TGA). This chapter describes the validation of TGA results and how the TGA results are treated to obtain kinetic parameters. It is concluded with the obtaining the kinetic rate equations for asphaltenes and slurry char gasification.

1.5 Objectives

The aim of this work is to study the pyrolysis of coal/asphaltenes slurry as well as the pyrolysis of asphaltenes in an atmospheric entrained flow drop tube furnace. The following detail analyses would be performed in the course of this thesis:

- The reactivity of chars obtained from the fast pyrolysis would be measured and the effect of temperature, heating rate and residence time on the produced char reactivity would be investigated.
- The characteristics and the structure of asphaltenes and slurry chars including morphology, particle size distribution and surface area would be determined.
- Kinetic study of the gasification of the asphaltenes and slurry chars with O_2 would be studied and a the reaction kinetic parameters would be found based on the TGA results

CHAPTER 2

Literature Review

2.1 Asphaltenes

Asphaltenes are the heaviest part of crude oil. They are high in aromaticity, polarity and molecular weight. Figure 2-2 illustrates the polarity, aromaticity and molecular weight of C₅ and C₇ asphaltenes. Asphaltenes that are precipitated in contact with n-C₅, are called C₅ asphaltenes and those that are precipitated in C₇ are called C₇ asphaltenes.

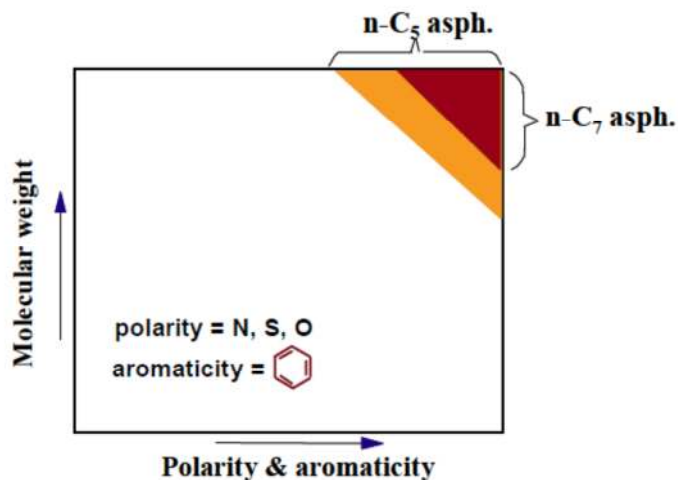


Figure 2-1 - "Long diagram" showing high polarity, aromaticity and molecular weight of asphaltenes (1)

Table 2-1 summarizes the properties of asphaltenes from different origins including Fosterton and Neilburg in Saskatchewan and Athabasca (used in the current work) in Alberta, Canada, San Fernando in Columbia and Orimulsion in Venezuela. As can be seen, asphaltenes generally contain very low ash (mostly less than one percent), but are high in volatile matter and fixed carbon. The sulfur content of the asphaltenes varies based on the origin of asphaltenes and the H/C ratio is around one due to it is being composed of mostly aromatic components.

Table 2-1 Typical properties of asphaltenes from various origins

	Fosterton⁽⁴⁾	Neilburg ⁽⁴⁾	San Fernando ⁽⁵⁾	Orimulsion⁽⁶⁾	Athabasca
<i>Proximate Analysis (wt.%)</i>					
<i>Volatile matter</i>	23.9	61.5	78.89	58.18	61.72
<i>Fixed Carbon</i>	75.1	38.1	19.89	12.84	37.88
<i>Ash</i>	0.88	0.39	0.53	0.18	0.40
<i>Ultimate Analysis</i>					
<i>C</i>	55.4	82.6	81.1	84.28	80.3
<i>H</i>	5.2	7.8	8.62	10.33	8.0
<i>N</i>	0.5	1.1	1.01	0.64	1.2
<i>S</i>	1.7	6.5	4.29	3.95	8.2
<i>O</i>	37.2	2	4.39	0.55	2.5
<i>H/C</i>	1.1	1.1	1.3	1.5	1.2

Athabasca asphaltenes are the feedstock in the current work. Asphaltenes as well as coal-asphaltenes slurry are used for pyrolysis experiments. Because in pyrolysis experiments the feed is sprayed into the reactor to form fine droplets, the viscosity of liquid and slurry feeds is very important in the feeder and spray design in order to get droplets with the desired quality.

2.2 Rheology of asphaltenes and slurries

2.2.1 Asphaltenes viscosity

The viscosity of asphaltenes depends strongly on the temperature. The modified Vogel-Tammann-Fulcher (VTF) equation which is a modified Arrhenius model is usually used to predict the asphaltenes viscosity as a function of temperature:

$$\eta = \eta_{\infty} \exp\{D/[(T/T_0) - 1]\} \quad (2-1)$$

where T_0 is the temperature at which the viscosity shows its low-temperature divergence and η_{∞} is the viscosity at $T=\infty$, according to Sirota (7). This model can predict the temperature dependent viscosity for a wide range of hydrocarbons including crudes, residues, lubes, deasphalted oils, solvents etc. Figure 2-22-2 shows the variation of the viscosity of Canadian bitumen asphaltenes vs. temperature (7).

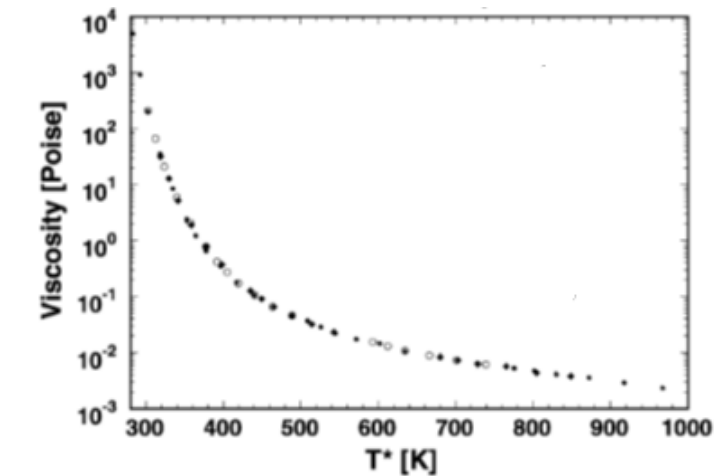


Figure 2-2 - Viscosity of asphaltenes from Canadian bitumen (7)

2.2.2 Viscosity of slurries

In slurries, the interactions between solid particles and the carrier fluid play an important role in determining the slurry properties. Interfacial tension and viscosity are two important characteristics of slurries. Because of more surface area and friction between particles and the fluid within the slurry, the interfacial tension of the slurry is greater than that of pure carrier fluid. Also, fine particles result in higher viscosity in slurries because of more inter-particle interactions. In such slurry with fine particles, more force is needed to deform the slurry for pumping or atomization applications.

According to Figure 2-3, the coal-water slurry shows a pseudo-plastic and shear-thinning behaviour. This pseudo-plastic behaviour can be described by a Bingham model as shown in the equation 2-2.

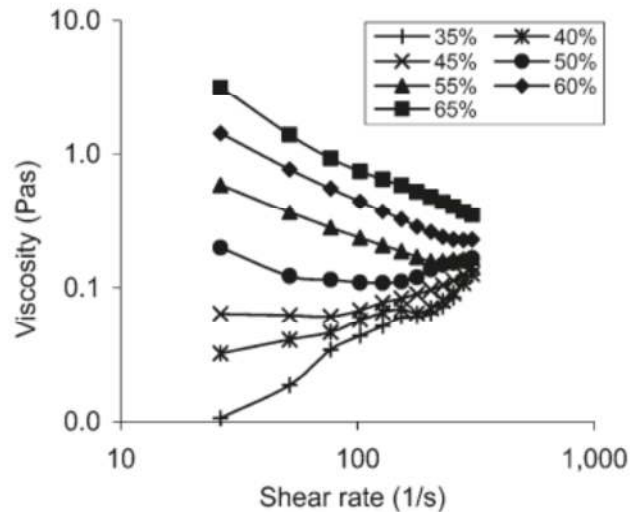


Figure 2-3 Effect of the solid loading on the shear rate to viscosity profile in coal-water slurries (particle size of 250-500 μm) (8)

$$\tau = \tau_y + K\dot{\gamma}^n \quad (2-2)$$

The maximum solid content of the slurry depends on its particle size. When the solid content of the slurry exceeds from a limit, the particles agglomerate and the carrier fluid will be trapped between the particles resulting larger particles in the slurry. It has been reported that coal-water slurries can be pumped with solid content of as high as 70%. Moreover, according to the observations, non-Newtonian behaviour of slurries will change from shear-thinning to shear-thickening by increasing the solid content (8). This change of the behaviour is shown in Figure 2-3.

2.3 Slurry atomization

2.3.1 Principles of atomization

The process of generating fine droplets is called atomization or spraying. This typically begins with forcing a fluid through a nozzle. The mechanisms of spray formation are considered to be very complex. According to the literature, there are two mechanisms for droplets breakup. The first mechanism is the breakup of a liquid core into droplets (figure 2-4). This mechanism is called the primary breakup, which is characterized by droplet size and the breakup length. The breakup length is the length of the intact liquid core before breaking up. In the second mechanism (i.e. secondary breakup), after formation of droplets large aerodynamic forces deform and break the droplets into fine droplets. The size of the droplets

characterizes the secondary breakup. Both liquid and surrounding atmosphere properties affect the size of droplets.

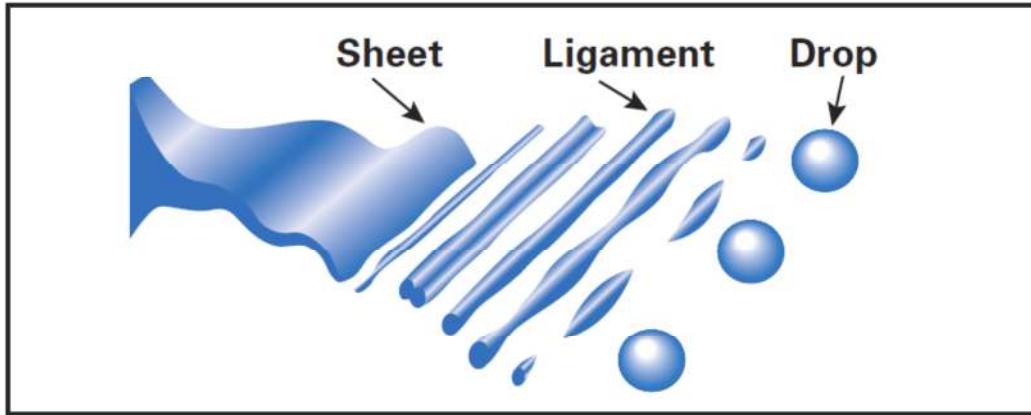


Figure 2-4 - Droplet formation steps

2.3.2 Primary Breakup

Depending on the fluid properties and the initial velocity, the primary breakup process may occur in one of four classified regions shown in figure 2-5. Droplet viscosity and surface tension as well as the intact core liquid velocity are key parameters in classification of the primary breakup regions. Those parameters are summarized in two dimensionless numbers including Ohnesorge and Weber numbers to better define the primary breakup.

Ohnesorge number determines the ratio of the viscose force to the surface tension force:

$$Oh = \frac{\mu_l}{\sqrt{\sigma \rho_l D}} \quad (2-3)$$

where μ_L and ρ_L and σ are the liquid viscosity, density and surface tension, respectively. The Ohnesorge number can also be written as follows.

$$Oh = \frac{\sqrt{We}}{Re_l} \quad (2-4)$$

The We number is the ratio of the inertial (i.e. aerodynamic) and surface tension forces.

$$We = \frac{u^2 D \rho_l}{\sigma} \quad (2-5)$$

where ρ_l and σ are density and surface tension of the fluid, respectively. D is the nozzle diameter and u is the liquid jet velocity.

The Reynolds number for the nozzle is defined as:

$$Re_l = \frac{u D \rho_l}{\mu_l} \quad (2-6)$$

where u is the liquid jet velocity.

In the atomization zone, breakup occurs at the nozzle tip, thus, the intact length is zero.

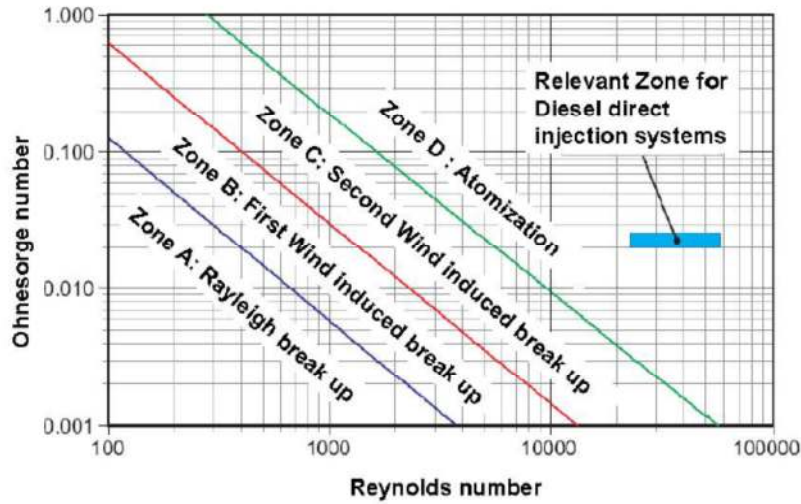


Figure 2-5 - Primary breakup regimes (9)

2.3.3 Secondary Breakup

Droplets that are formed during primary breakup are exposed to two major forces including droplet inertia (disruptive force) and surface tension. To quantify the breakup of droplets in the secondary breakup process, the same dimensionless numbers are used. The Weber number is defined based on d (droplet diameter) and u_{rel} is relative velocity of droplet with respect to the surrounding atmosphere.

$$We = \frac{u_{rel}^2 d \rho_g}{\sigma} \quad (2-7)$$

where ρ_g is the density of the ambient fluid. A large We number means a higher tendency towards breakup. Moreover, droplet viscosity is important in the secondary atomization process. The viscosity of the droplet hinders droplet deformation and dampens the energy of inertial force. Oh number

relates the viscose forces to the surface tension force and shows the likelihood of fragmentation:

$$Oh = \frac{\mu l}{\sqrt{\sigma \rho l d}} \quad (2-8)$$

According to the literature (9), droplet viscosity forces have significant effect when $Oh > 0.1$. If Oh number is below 0.1 the breakup process is independent of the viscosity forces. It is worth mentioning that decreasing the droplet diameter increases its surface tension, therefore, higher velocity required to break up the droplet. Again, there are different breakup patterns for secondary atomization that are shown in Figure 2-6.

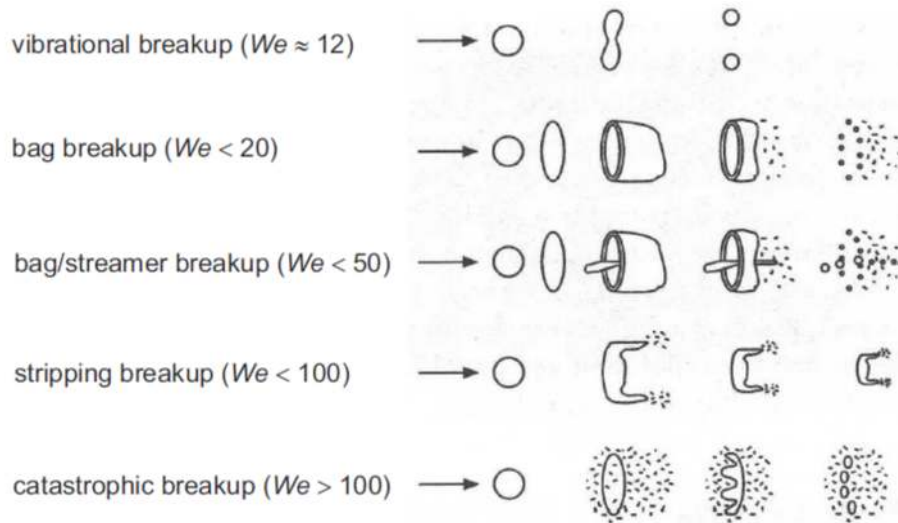


Figure 2-6 - Secondary breakup regimes (10)

2.3.4 Droplet size distribution

The image is generated on the detector by transmitting the laser to the spray as shown in Figure 2-7.

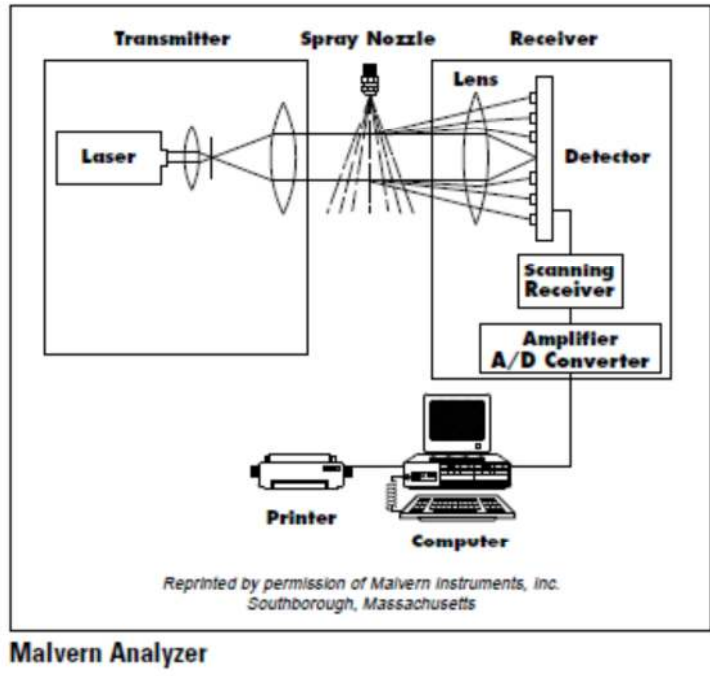


Figure 2-7 - Schematic of a particle size analyzer (Courtesy of Malvern (11))

Data analysis is carried out using mathematical and statistical methods. In order to quantify the droplet and particle size distributions, Sauter mean diameter (SMD) is used to interpret the data obtained by the detector. SMD is the ratio of particle volume to surface area of a distribution:

$$d_{32} = \frac{\int_0^{D_{max}} d^3 f_n(d) d(d)}{\int_0^{D_{max}} d^2 f_n(d) d(d)} \quad (2-9)$$

In the above equation, $f_n(d)$ is the number function of droplets obtained by the detector (12).

2.3.5 Types of sprays

There are various types of sprays designed for different applications including orifice nozzle, pressure swirls atomizer, tangential flow spray, twin-fluid atomizer, internal and external mixing atomizers, etc.

In two fluid atomizers, the liquid or slurry is mixed with the spraying gas either before approaching the nozzle tip (internally mixed) or right at the nozzle tip (externally mixed). Effervescent atomizers are a type of internally-mixed atomizers used widely in industry. In effervescent atomizers, a bubbly two-phase flow is formed by gas injection and then fine droplets are generated at the nozzle exit by rapid expansion of the bubbles. Figure 2-8 schematically shows the mechanism of fine droplets generation in effervescent atomizers.

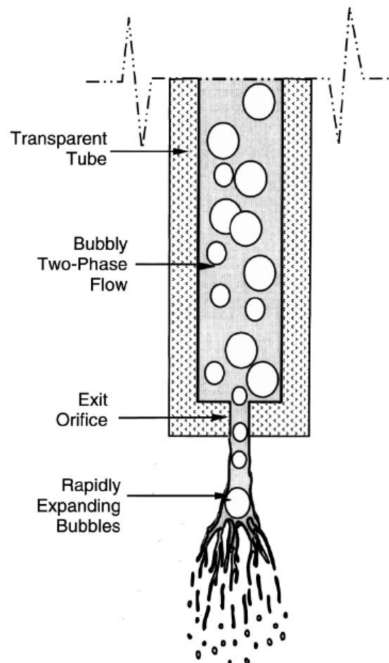


Figure 2-8-Schematic of an effervescent atomizer (12)

Air to liquid ratio (ALR) is an important factor influencing the droplet size distribution of a spray. Obviously, increasing the ALR decreases the SMD since it will be easier to overcome the surface tension and viscous forces with higher gas velocities. Bunckner *et al.* (13) studied the dependency of SMD and ALR and the operating pressure for effervescent atomization of coal-water slurries. They reported that SMD of the atomizer increased with ALR and was independent of the slurry type (between coal-water slurries). Doohar J. (14) obtained a phenomenological model for Sauter mean diameter of viscous fluids and coal slurries as follows:

$$SMD = a^2 \frac{10^4 \sqrt{Z}}{\sqrt{\Sigma}} We^{-1.09} \quad (2-10)$$

where a is the nozzle diameter, Σ is the cross section of the spray and $Z = \sqrt{We/Re}$. In case of coal-water slurry, the correlation was as follows:

$$SMD = 1.28 \times 10^8 \frac{a}{\Sigma} We^{-1.68} \quad (2-11)$$

It is shown that variation of SMD with We number for viscous fluids is not that fast and the droplet size is proportional to the square root of the viscosity of the fluid (14). Son and Kihm (15) investigated the effect of coal particle size on the coal-water slurry atomization. According to them, the interfacial tension of slurry is higher than the pure fluid. Furthermore, the viscosity and interfacial tension of the slurry was shown to increase by decreasing the mean diameter of the particles, due to the availability of more surface between particles and the fluid. They described that in order to

atomize the slurry, the spray should overcome the capillary forces of the fluid stuck between the solid particles. Since the capillary force is inversely related to the particle diameter, larger particles in the slurry exhibit weaker capillary forces. Thus, the quality of spray of slurries with relatively larger particles is usually better. In droplets from slurry with smaller particles, few solid particles was found to be trapped and the droplets were larger. On the other hand, droplets from slurry with larger particles were smaller and contained mostly one or two solid particles.

2.4 Pyrolysis and gasification of slurries

2.4.1 Coal-water slurry gasification

Many research works have been conducted on coal-water slurry gasification across the world. Thus, this type of feed is well studied from various aspects and its characteristics including viscosity, feeding systems, the hydraulic design of slurry feeding is also well defined.

Choi *et al.* (16) studied the coal-water slurry gasification in a 1 ton per day coal-water slurry oxygen blown entrained-flow gasification. They used different types of coal including Australian, Indonesian and Chinese coals. The gasifier consisted of a burner at the top, the main reaction zone and a slag quenching part at the bottom. The operating temperature was in the range of 1300-1550 °C and the operating pressure was between 0-5 atm. They used a 65% coal-water slurry with viscosity of about 450-1520 cP. In

the liquid and slurry feeding systems, the viscosity of the feedstock is very important because the spray should convert to fine droplets for pyrolysis and gasification. Figure 2-9 shows the variation of coal-water slurry viscosity with coal concentration. Since adding coal increases the viscosity exponentially, Choi *et al.* added a surfactant to the slurry to reduce the viscosity and improve the feeding quality. Moreover, they studied the gasification performance of coal-water slurry with different O_2 /coal ratios. They reported the effect of O_2 /coal ratio on syngas composition, heating value and cold gas efficiency. According to their results, the optimum operating condition for O_2 /coal ratio is around 0.9.

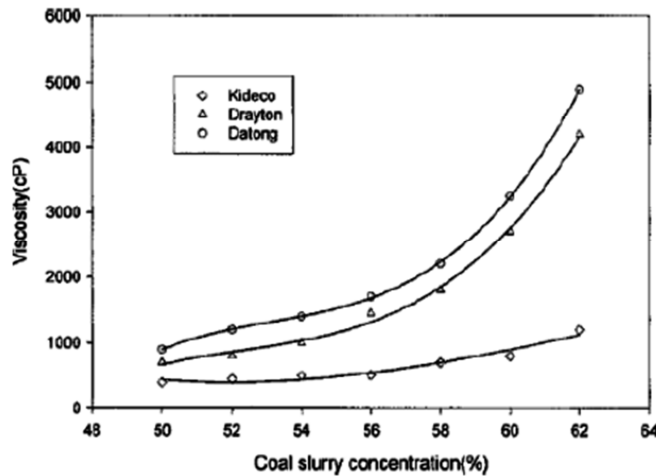


Figure 2-9 – Coal-water slurry viscosity vs. coal concentration (16)

2.4.2 Bio-oil and biomass slurry pyrolysis and gasification

Sakaguchi *et al.* (17) studied the steam gasification of bio-oil and bio-oil/char slurry in an atmospheric lab-scale fluidized bed reactor with catalytic and non-catalytic bed material. Both bio-oil and char were produced from a commercial wood biomass pyrolysis plant. They used a naphtha steam reforming catalyst contained nickel as the packing material. In order to feed bio-oil and bio-oil/char slurry, they implemented a pre-built airbrush nozzle (Pasche Airbrush Co.) in one side of the reactor to spray the feed. According to their design, the spray consisted of annular tubes through which atomizing gas (N₂) was fed into the outer tube and the slurry was fed into the inner one.

They showed that using the catalysis in steam gasification leads to higher H₂ yield and carbon conversion and lower CO yield in the syngas. Moreover, the authors reported that in non-catalytic steam gasification CO and CO₂ yield increased by increasing temperature up to 830 °C. On the other hand, the gasification temperature did not affect the CO and CO₂ yield in catalytic reactions. They also found that for both conditions of catalytic and non-catalytic steam gasification, carbon conversion was much lower in slurry gasification rather than in non-slurry bio-oil gasification. In another work, Sakaguchi *et al.* (18) studied the reactivity of char from pyrolysis of bio-oil/char slurry. This work will be more discussed in chapter four. Kolb *et al.* (19) conducted experiments on biomass-based slurries in an atmospheric entrained flow gasifier to produce tar-free synthetic gas. They aimed to find

the optimum design for a high-pressure entrained flow gasifier for the same feedstock at 40-80 bar. In their experiments, the bio-oil feedstock was prepared in a separate fast pyrolysis process from biomass. Then, in the gasification process, bio-oil was atomized into the reactor using a custom-designed atomizer with oxygen as both atomizing and gasifying agent. They studied the effect of fuel composition and atomization quality on the gasification performance and conversion efficiency at temperatures around 1200 – 1500 °C. In some experiments with ethylene glycol and oxygen, they showed that the pyrolysis and gasification performance is strongly dependent on the atomization quality. They also showed that atomization with air provides better quality than oxygen-enriched air (50% O₂). In the former case, lower temperature on the axis of the spray was found due to higher evaporation rate. Moreover, soot and tar formation on the jet axis during gasification caused an unrealistic measurement of C/H. Zhang *et al.* (20) studied the pyrolysis and gasification of a bio-oil from fast pyrolysis of sawdust at 500 °C in a fluidized bed reactor. The pyrolysis part of their work has been conducted using the TGA at the heating rates of 5, 10 and 20 °C/min up to 900 °C. They reported that devolatilization step in bio-oil pyrolysis took place in the temperature range of 50-120 °C. At this stage, the sample lost moisture as well as some light hydrocarbons such as aldehydes, organic carboxylic acid and alcohols. According to the authors, the second stage of bio-oil pyrolysis occurred at temperatures above 200 °C. At this stage, phenols, eugenol and vanillin compounds that were released at the first step

were cracked. At higher temperatures, the release of organic compounds decreased while the content of CO, CO₂ and CH₄ increased because of cracking of heavier components. bio-oil was completely converted at 1000 °C. Zhang et al. (20) also conducted gasification of bio-oil in a fixed bed gasifier. Because of the high content of elemental oxygen in the bio-oil, this work was carried out in the absence of gaseous oxygen. Figure 2-10 shows the variation of syngas composition with temperature in this work.

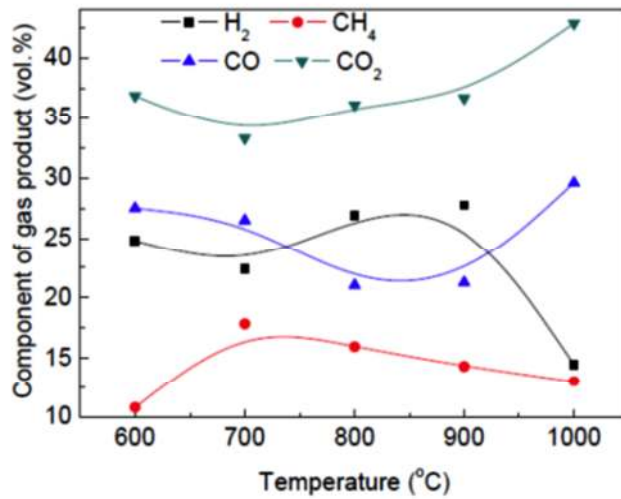


Figure 2-10 - Syngas composition from bio-oil gasification at different temperatures (20)

According to Figure 2-10, CO₂ content of the syngas was much higher than the other components and it increased continuously with temperature. The authors postulated that high carboxylic acids in the bio-oil might be the source of CO₂ in the syngas. Furthermore, CO content decreased with

increasing the temperature up to 850 °C and after that, it increased with temperature.

2.5 Asphaltenes and heavy oil pyrolysis and gasification

There are relatively more published works on asphaltenes pyrolysis compared to the asphaltenes and heavy oil gasification. Liu *et al.* (21) studied the pyrolysis of asphaltenes with the aim of characterizing tar, char and gases. The asphaltenes they used were extracted from Chinese coal. The pyrolysis experiments carried out with a thermo balance. They characterised the tar as alkanes in the range of C₁₂-C₃₁ as well as polycyclic aromatics. Below 400 °C, they did not observe any gas formation except CO₂. Formation of CO₂ was attributed to the presence of carboxylic acid anhydrides in the feedstock. They observed a peak in the gas formation at temperatures between 400-600 °C. At temperatures above 600 °C, the structure of asphaltenes was found to be completely broken down to char. Zhao *et al.* (22) investigated the effect of reaction time and temperature on asphaltenes pyrolysis in a molten bath reactor. They used asphaltenes derived from Athabasca bitumen. They reported that pyrolysis and cracking of asphaltenes happened at around 400-550 °C.

They found a multi-stage reaction of the pyrolysis of asphaltenes consisting of five steps as follows:

1. Dealkylation of side aliphatic chains and decomposition to polar compounds and free radicals according to Figure 2-10.

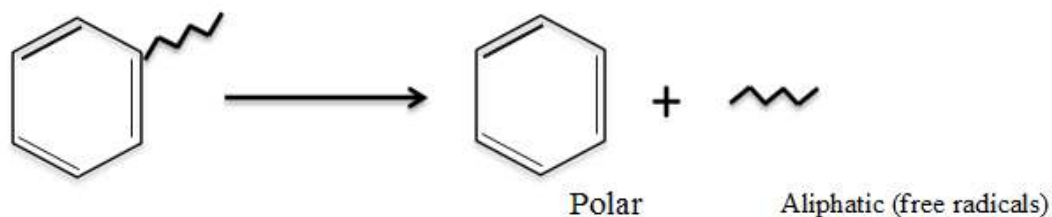


Figure 2-11 - Dealkylation of side aliphatic chains

2. Polymerization of free radicals generated in the first step and combination of rings which results in formation of larger molecules.
3. Dehydrogenation of rings.
4. Crystallization of alkyl chains. Steps 3 and 4 reduce H/C ratio in the solid residue.
5. Condensation and pre-condensation of aromatic compounds. The components containing heteroatoms were found to go in the carbon residue.

As mentioned before, there are a few published works on asphaltenes and heavy oil gasification. Ashizawa *et al.* (6) studied the gasification characteristics of extra heavy oil in a lab-scale gasifier with a capacity of 2.4 ton/day. Their feedstock was Orimulsion, which is a bitumen-based fuel from Orinoco Belt in Venezuela. The set up consisted of a pressurized (1.9 MPa)

entrained flow type gasifier, a raw-gas cooler and, 15 m³ feedstock storage tank along with a supply system. They used oxygen as the gasifying agent with oxygen ratio in the range of 0.37 to 0.41. They found that increasing the oxygen ratio leads to increase of carbon conversion while it reduces the cold gas efficiency (CGE) and caloric value of products. According to this research, the HHV wet values were in the range of 9.5-10.5 MJ/m³ and CGE was about 75-80% and carbon conversion was more than 97%. They collected char and gas samples at different levels of the gasifier and found that high conversion was reached at the top 1/3 of the reactor. Also, gas analyses revealed that CH₄, H₂O and CO concentrations decreased along the gasifier while H₂ and CO₂ concentrations increased.

Moreno *et al.* (5) investigated gasification of Colombian asphaltenes with oxygen in a batch process. The objective of their work was to find a relationship between syngas compositions and gasification temperature and oxygen percentage as the gasifying agent. Their feedstock was asphaltenes of San Fernando crude oil from Columbia. It was obtained from a deasphalting unit with 8.7 °API. The asphaltenes sample (15 gr) was placed in a horizontal tubular oven and heated up to 1000 °C. The continuous flow of O₂ diluted with Ar at 170 psi (11.6 atm) was supplied as the gasifying agent. The authors conducted semi-batch gasification experiments at temperatures in the range of 900 to 1000 °C. They concluded that increasing the temperature improved the syngas composition (i.e., quality) and carbon conversion since gasification at higher temperatures decreases the amount of tar and other

by-products. Also, they reported that higher temperature increased CO and H₂ content in the syngas while it decreased CO₂ and CH₄, which is favorable in gasification syngas. Moreover, at higher gasification temperatures, the higher H₂/CO ratio in the syngas attained with less oxygen as the gasifying agent. Finally, they found more sulfur compounds in the syngas at higher temperatures. They postulated that this could be attributed to breaking down the heavier molecules at higher temperature.

2.5.1 Asphaltenes char characteristics

Liu *et al.* (21) revealed a relationship between the ratio of heteroatoms in the original asphaltenes feedstock and the char surface area in a sense that the more the heteroatoms in the original feedstock (i.e. $[(O)+(N)+(S)]/[C]$), the larger the char surface area. According to them, chars obtained at atmospheric condition were anisotropic while those were obtained at vacuum condition were isotropic. Also, Ashizawa *et al.* (6) collected char samples from extra heavy oil at several height of a pressurized entrained flow gasifier. Figure 2-12 shows char samples they collected with oxygen ratio about 0.37 at two different heights. They observed that during gasification the number of holes on the surface of the char particles was increased.

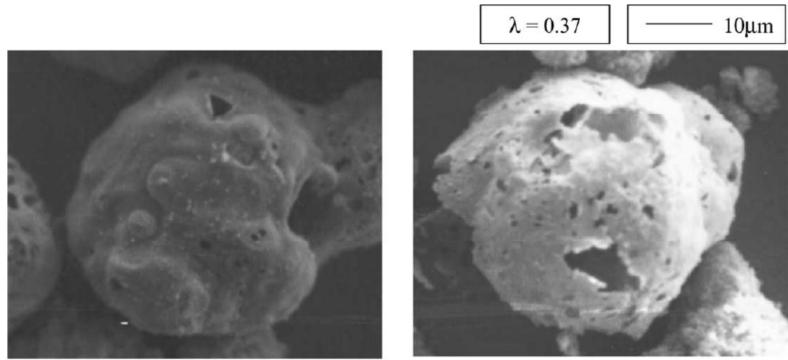


Figure 2-12 - Char samples from Orimulsion extra heavy oil (6)

Fouga *et al.* (23) prepared char from asphaltite, which is similar to asphaltenes, in a fixed-bed reactor. Figure 2-13 shows the SEM images of asphaltite char. The authors did not observe much porosity on the surface of the chars. Also, low BET area proved that observation.

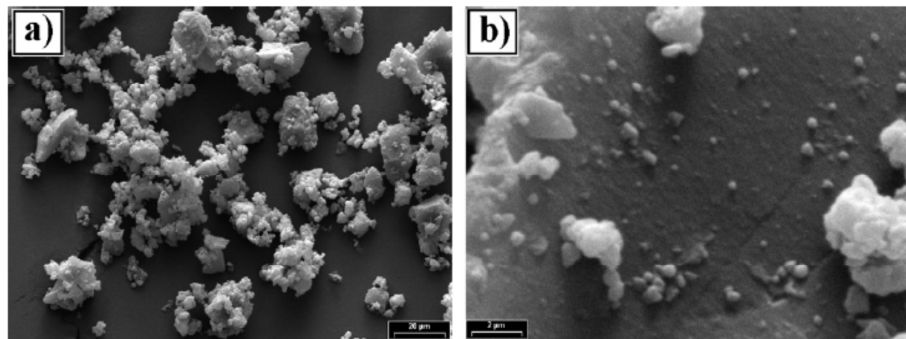


Figure 2-13 - SEM images of the char from asphaltite (23)

2.6 Kinetics of asphaltenes gasification

2.6.1 Analysis of the mass transfer effect

The overall chemical reaction rate of a char particle depends not only on the intrinsic chemical reaction rate but also on the mass transfer from the bulk to the surface and to the pores of the particle. In other words, the reactant gas concentration on the surface of the particle is not the same as the bulk concentration because of mass transfer diffusion. Therefore, the mass transfer resistance determines the local concentration of reactant gas on the surface or within the pore structure of the particle. Figure 2-1414 shows how the diffusion affects the local gas concentration.

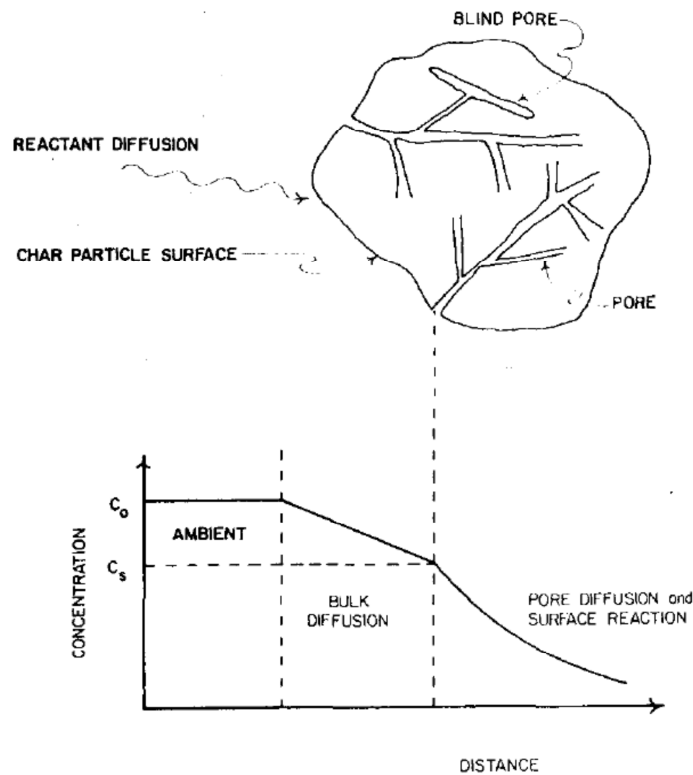


Figure 2-14 - Concentration profile for the reactant gas close to a char particle (24)

For kinetic study of heterogeneous reactions with TGA, the mass transfer effect should be kept negligible. Thus, the heterogeneous reaction is controlled by chemical reaction rate and not the mass transfer diffusion. This is called the intrinsic reaction rate and is independent of char porosity, reactant gas flow rate, and sample size and mass. The intrinsic reaction rate is usually defined as:

$$\hat{R} = kP_i^n \quad \text{g.carbon/m}^2.\text{s}$$

where \hat{R} is intrinsic reaction rate, k is exponential factor, P_i is partial pressure of the reactant gas and n is the order of reaction with respect to reactant i .

The intrinsic reaction rate also can be defined based on the concept of active sites. The active site theory assumes that the reactions take place at some active sites on the surface. In the case of char reactions, potential active sites are (24):

1. carbon edges or dislocations
2. inorganic impurities
3. oxygen and hydrogen functional groups

According to this theory, the reaction involves three steps including:

- a) adsorption of reactant gas on the surface by chemisorption
- b) surface reaction
- c) product(s) desorption

The overall reaction rate is defined based on the intrinsic rate as $R_m = \eta A \hat{R}$, in which η is effectiveness factor that represents the fraction of the surface area required for reaction if the local intrinsic rate was \hat{R} .

Figure 2-155 shows the concentration profiles of the reactant gases inside ($<R$) and outside ($>R$) of a porous particle. Curve I depicts the case for which the chemical reaction rate is slow compared to the mass diffusion. Therefore, the concentration is the same along the path. In this case, the process is assumed to be chemically controlled. As the intrinsic reaction rate \hat{R} increases, the mass transfer diffusion cannot keep up with the chemical rate which leads to profiles a, II, a', b, IV and finally III. In those regions, mass transfer controls the whole process.

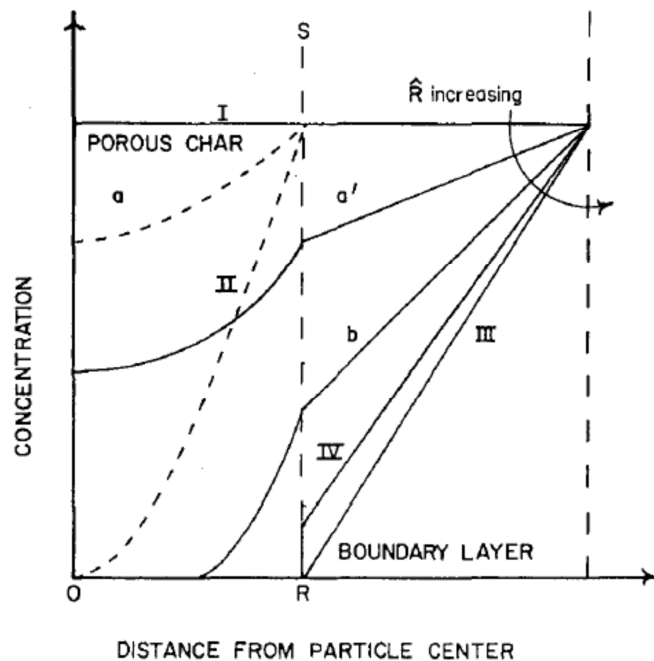


Figure 2-15 - Reactant gas profiles external and internal to a porous char particle (24)

In curve III, the chemical rate within in the pore is rapid compared to the diffusion that all the reactant gas is consumed in the pores and on the surface so the process is completely controlled by mas transfer diffusion. Generally, for the case of intrinsic kinetic reaction the profile is sililar to either curve I or IV. In the latter case, the chemical rate is fast enough to consume the reactant close to the surface therefore the overall reaction is controlled by the chemical reaction.

Regarding the described mass transfer effect, before any heterogeneous kinetic study, one should make sure that the overall reaction is chemically controlled with negligible mass transfer effect. Chemical reactions at high temperatures usually are controlled by mass transfer since the intrinsic chemical rate is faster than the mass transfer diffusion. Thus, the effect of mass transfer at high temperatures should be removed by increasing the reactant gas flow rate and decreasing sample size and weight.

In kinetic studies with thermogravimetric analyzer (TGA), usually a few experiments are needed in order to find the good condition in which the overall reaction is chemically controlled and the diffusional mass transfer is negligible. The typical method for this purpose is to measure the reaction rate at high temperatures with different purge gas flows and sample weights. The reaction rates then could be compared to each other to check whether it is affected by changing the reactant gas flow or sample weight. As mentioned

before, if it is chemically controlled, the reaction rate will not be changed with gas flow or the sample size.

2.6.2 Effect of heating rate

Murugan *et al.* (25) studied the thermal behaviour of Fosterton asphaltenes (from Saskatchewan, Canada) using non-isothermal TGA experiments with different heating rates up to 800 °C. In their research, air was used as the oxidative agent. The objective of their study was to obtain a kinetic equation for pyrolysis of C₅ Fosterton asphaltenes. The authors used a distributed activation energy model (DAEM) to analyse the pyrolysis reactions. The model assumes an infinite number of first order parallel reactions with various activation energies occurring during the non-isothermal experiments. They proposed a method to estimate the normalized distribution curve of activation energies $f(E)$ and $k_0(E)$ by using a set of three TGA curves. The following equation shows the presented distribution of activation energies when it applies to the change in total volatiles.

$$1 - \frac{V}{V^*} = \int_0^{\infty} \exp\left(-\int_0^T \frac{k_0}{a} e^{-\frac{E}{RT}} dt\right) f(E) dE \quad (2-12)$$

where V/V^* is the total conversion of volatiles at temperature T , $f(E)$ is the distribution function of activation energies of multiple first order reactions and a is the linear heating rate of the pyrolysis reaction. The simplified form of the above equation is:

$$\frac{V}{V^*} = 1 - \int_{E_S}^{\infty} f(E)dE = \int_0^{E_S} f(E)dE \quad (2-13)$$

According to the authors, the Arrhenius equation in the simplified form can be described as:

$$\ln\left(\frac{a}{T^2}\right) = \ln\left(\frac{k_0R}{E}\right) + 0.6075 - \frac{E}{RT} \quad (2-14)$$

Using the last equation and the plot of $\ln(a/T^2)$ vs. $1/T$, both activation energy and k_0 can be obtained for different heating rates (i.e. a).

During their experiments, they found that 425 °C is the optimum temperature for producing coke since coke yield decreases with increasing temperature. Also, they showed that as pyrolysis temperature increased, the H/C ratio decreased. Consequently, the reactivity of cokes that is related to H/C ratio decreased. To justify this phenomenon, they assumed that chars obtained at higher temperatures contain more condensed structure compared to those obtained at lower temperature. This assumption is in accordance with the proposed pyrolysis steps by Zhao *et al.* (22). Furthermore, their results showed that the coke yield decreased with increase of temperature and the heating rate. It can be said that the more severe the pyrolysis condition is, chars obtained with the lower yield and the lower reactivity. Finally, they obtained activation energy and the pre-exponential factor of 93.46 kJ/mol and $9.59 \times 10^5 \text{ min}^{-1}$ respectively.

Murugan *et al.* (25) observed that increasing the pyrolysis heating rate increases the temperature with maximum rate of decomposition. In a recent study, Fouga *et al.* (23) conducted thorough experiments on kinetics of CO₂ gasification of Argentinian asphaltite at temperatures between 775 to 950 °C. Like asphaltenes, asphaltite has low ash and high carbon content and it is a good source for syngas production. They used both non-isothermal and isothermal methods with thermal gravimetric analyzer (TGA). The authors obtained chars by pyrolysis of asphaltite in a fixed bed reactor. Further, non-isothermal TGA experiments showed that 820 °C was the starting temperature of gasification.

The authors assumed the chemical reaction rate as:

$$r = \frac{d\alpha}{dt} = G(\alpha) \cdot K(T) \cdot F(P_i) \quad (2-15)$$

$$\int \frac{d\alpha}{G(\alpha)} = g(\alpha_i) = K(T) \cdot F(P_i) \cdot t_i \quad (2-16)$$

where α_i is the conversion at a given time and $K(T)$ is the temperature functionality in the form of Arrhenius equation. The rate equation can be rearranged as:

$$g(\alpha_i) = k_0 \exp(-E/RT) \cdot F(P_i) \cdot t_i \quad (2-17)$$

$$\ln t_i = \ln \left[\frac{g(\alpha_i)}{F(P_i) \cdot k_0} \right] + \frac{E}{RT} \quad (2-18)$$

For a given α_i :

$$\ln t_i = cte + \left(\frac{E}{R}\right) \cdot \frac{1}{T} \quad (2-19)$$

The first term at the right hand side was constant if conversion and partial pressure were held constants. In this case, t_i was the time at which the reaction reached to a particular conversion. So plotting $\ln t_i$ vs. $1/T$ gave the intrinsic activation energy of the reaction.

2.6.3 Effect of partial pressure

Fouga *et al.* (23) tried gasification with CO₂ at partial pressures between 10 and 80 kPa in order to observe the effect of CO₂ on gasification rate of asphaltite char and to find the reaction order with respect to CO₂ partial pressure. They considered the $F(P_i)$ function as $B \cdot P_{CO_2}^n$. The first equation integrated and rearranged to reach the following equation:

$$-\ln(t)_i = H(\alpha_i) + n \ln P_{CO_2} \quad (2-20)$$

where t_i is the time at which the reaction reaches to the conversion degree of α_i at temperature T . The slop of the plot of $\ln(t_i)$ vs. $\ln(P_{CO_2})$ gave the order of reaction with respect to CO₂ partial pressure. The authors calculated the reaction order of 0.5 in this case. According to them, no gasification studies on asphaltite were available in that time to compare the results; nonetheless, the calculated reaction order was in the range of the reaction orders of bituminous coal with CO₂.

Finally, Fouga *et al.* (23), found the equation rate for CO₂ gasification of asphaltite as:

$$Rate = \frac{d\alpha}{dt} = (1 - \alpha)^{2/3} \cdot 1.1 \times 10^5 \exp\left(-\frac{185 \frac{kJ}{mol}}{R.T}\right) \cdot P_{CO_2}^{0.5}$$

In a further work, Sakaguchi *et al.* (18) studied the kinetics of steam gasification of char from rapid pyrolysis of bio-oil/char slurry. This study was a part of their work on steam gasification performance of bio-oil/char slurry, which mentioned before in this chapter (17). As mentioned, char and bio-oil were from the same source. The details of their work was presented here before. They used the power law model for the gasification equation rate as:

$$r = k_0 \exp\left(-\frac{E}{RT}\right) P_{H_2O}^n \quad (2-21)$$

The gasification experiments were carried out using TGA and at the temperatures between 900 to 1200 °C. They found the activation energy of 219±13 kJ/mol and $k_0=3.4 \times 10^5 \text{ s}^{-1} \text{ Pa}^{-n}$. They calculated the order of reaction with respect to the partial pressure of steam to be 0.34±0.14. They also reported that the reactivity of the char from slurry increased with the pyrolysis heating rate but it was lower than the reactivity of the original char from bio-oil.

Moreover, Mahinpey *et al.* (4) compared the kinetic and thermal behaviour of crude oils derived from Fosterton (as a medium oil) and

Neilburg (as a heavy oil) fields in Saskatchewan, Canada. The authors extracted C₅ asphaltenes from the crude oils and then obtained coke from asphaltenes using TGA with different heating rates up to temperatures 425, 500 and 550 °C. In order to observe the reactivity and thermal behaviour of the cokes they conducted isothermal and non-isothermal TGA oxidation experiments. The non-isothermal experiments carried out by rising temperature up to 800 °C. Also, the authors conducted oxidation at 375, 425 and 500 °C for the isothermal experiments. According to them, oxidation rate below 375 °C was very slow.

From coke formation experiments, they concluded that hydrogen was transferred from heavier components to the lighter ones while carbon was rejected from the lighter components to the heavier ones. Moreover, they reported that increasing pyrolysis temperature led to have less residual carbon. According to them, coke yield was about 25 – 60 wt.%. As reported by Zhao *et al.* (22), Mahinpey *et al.* (4) also found that heteroatoms remain and concentrate in char. They postulated that those heteroatoms act like an initiator to start coke (char) formation. Further, they found that by increasing the pyrolysis temperature, the temperature at which the oxidation rate is maximum, was increased. We can put this finding together with the similar finding of Murugan *et al.* (25) who observed that increasing the pyrolysis heating rate increases the temperature with maximum rate of decomposition.

CHAPTER 3

Pyrolysis Experiments

The results of the pyrolysis experiments with asphaltenes and asphaltenes/coal slurry feedstock are discussed in this chapter.

3.1 Experimental setup

Pyrolysis experiments and char collection carried out in an atmospheric entrained flow drop tube furnace shown in Figure 3-1. The setup consists of an electrically heated furnace with molybdenum disilicide heating elements (Moly-D33) with the maximum working temperature of 1800°C. The tube is made of Alumina with 6.5 cm ID and 153 cm height. The maximum allowable operating

temperature for the Alumina tube setup is limited to 1600 °C. Three PID temperature controllers (Omron E5CK) adjust the temperature along the reactor (the drop tube) in three different zones (i.e. top, middle and bottom). Three K-type thermo couples read the temperature at the same three zones along the tube. The PID controllers are connected to a computer that can remotely communicate with the controllers using LabView[®] interface. The feeding system consists of a slurry mixing vessel and stainless steel ¼" tubes to carry the feed to the reactor. Asphaltenes are solid at room temperature and need to be heated and molten before feeding to the reactor. Thus, the mixing vessel as well as all the tubes that carry asphaltenes were wrapped with electrical heating tapes and insulated with glass wool and fiberglass. The feed (i.e. liquid or slurry) was mixed using a magnet stirrer inside the vessel. The vessel was placed on a hot plate with stirrer and the top surface temperature set to 205°C for the purpose of heating and stirring. The problems associated with the sealing of mixer shaft in case of using an impeller for mixing was eliminated by using a magnet stirrer. The solid feeds (asphaltenes and coal) were put into the vessel when it was cold and then heated up to the melting temperature. Since asphaltenes form coke at higher temperatures, the temperature along the feeding system was strictly controlled to be kept lower than the coking temperature of around 320°C.

The mixing vessel was slightly pressurized with 4.8 purity nitrogen instead of using a pump. The flow of feed was calibrated with the pressure inside the vessel. Furthermore, after finishing the experiments and before leaving the system at high temperature over the night, the remaining asphaltenes in the

feeding tubes were removed by pressurized nitrogen in order to prevent coke formation within the tubes ending.

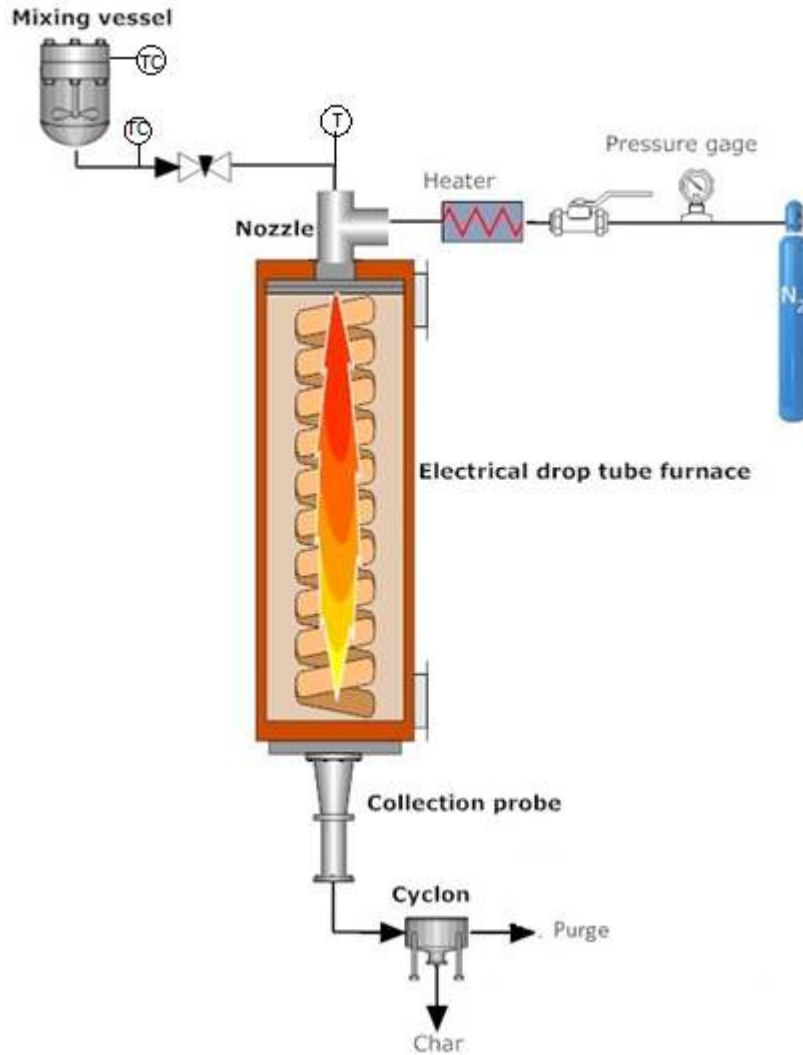


Figure 3-1 – Schematic diagram of the drop tube and the feeding system

The liquid or slurry feed was sprayed with nitrogen into the drop tube using a spray mounted at the top of the drop tube. The spray should have a narrow spray angle since the tube ID is rather small (6.5 cm), otherwise, the droplets would collide with the tube wall. In addition, the spray should be able to handle

low liquid flow rates. The spray was selected after trying various configurations with olive oil/coal slurry as the fluid (Figure 3-2). Finally, a spray which consists of annular tubes was selected to meet those two criteria. In this spray, the liquid passes through the inner tube and nitrogen (i.e. spraying gas) passes through the outer tube. Nitrogen is heated to 250°C before entering the nozzle using an inline heater. The nitrogen flow rate is adjusted using high precision mass flow controllers (AALBORG instruments).

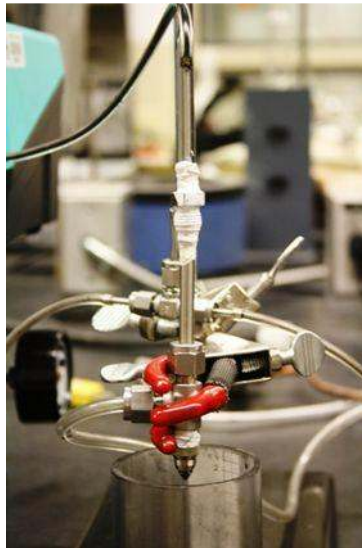


Figure 3-2 - Cold spray experiments with olive oil/coal slurry

Outlet gas and char particles were cooled down and collected at the bottom in an air-cooled collection probe. Following the collection probe, char particles are separated from the gas stream and are collected in a cyclone. Further, the flue gas is passed through a bag filter, which traps sub-micron particles. The pressure inside the drop tube is adjusted using a pressure difference controller (PDC). The PDC compares the pressure inside the reactor with the atmospheric

pressure and adjusts the inside pressure slightly (i.e. 0.02 psi) higher than the atmospheric pressure.

3.2 Fuel characterization

Asphaltenes from deasphalting unit of Nexen Inc. plant in Long Lake, northern Alberta, were used in this study. In this plant, the Asphaltenes are removed from Athabasca bitumen in the OrCrude™ unit. Table 3-1 shows proximate and ultimate analyses of asphaltenes. The proximate analysis was determined according to ASTM D7852 with thermal gravimetric analyzer.

Table 3-1 - Proximate and ultimate analyses of asphaltenes

Proximate analysis			Ultimate analysis				
FC	VM	Ash	C	H	N	S	O
37.88	61.72	0.40	82.70	7.42	1.15	7.96	0.77

Figure 3-3 shows the viscosity of asphaltenes feedstock used in this work. The viscosity measurement was carried out in the oscillatory mode using a controlled stress/strain Bohlin Gemini HR nano rheometer (Malvern Instruments Limited, U.K.). The configuration used was an extended temperature cell (ETC) parallel plate (25 mm) using a forced gas system to heat and cool the sample. The uncertainty in temperature measurements is estimated to be less than 0.2 °C, which contribute to a 2-3% uncertainty in viscosity.

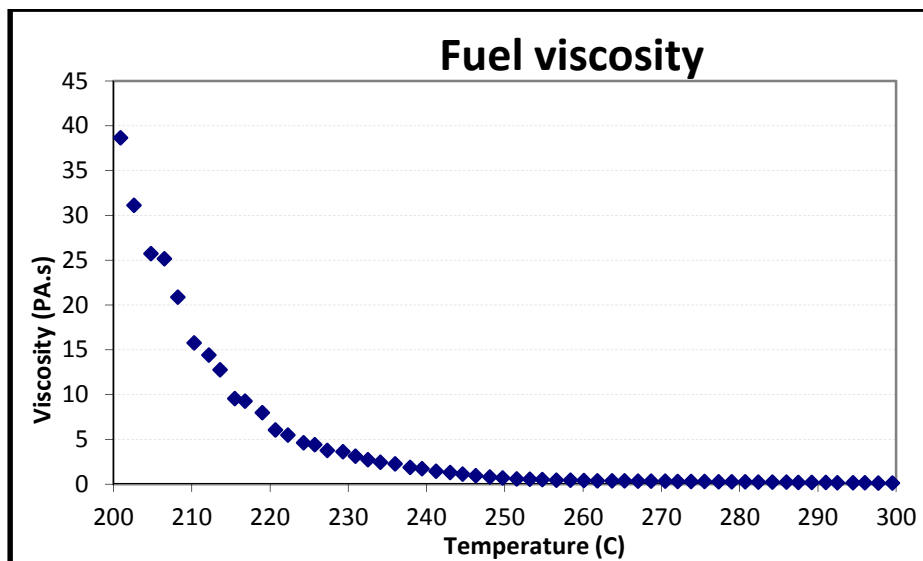


Figure 3-3 - Viscosity of the asphaltenes feedstock

3.3 Char preparation

Chars obtained from the asphaltenes pyrolysis experiments at five temperatures of 800, 1000, 1100, 1200, and 1400°C. Before starting the experiments, the furnace was heated up to the desired temperature overnight. The maximum heating and cooling rate was limited due to the construction material of the drop tube (i.e. Alumina). During the heating period, air with flow rate of 7 lit/min was passed through the tube. After reaching the desired temperature, air was switched to high purity nitrogen (99.99%) with the same flow rate in order to purge the system. The tube was kept for about 30 min in that situation to ensure that oxygen is completely purged out of the tube.

The feeding system was heated from the morning for about 3 hours depending to the amount of asphaltenes inside the vessel and the tubes. The vessel external temperature was set to 250°C and the external temperature of the tubes was set to 230°C because of the limitation in temperature rating of the valve (i.e. 240°C) used in the feeding system. A temperature reader displays the temperature of asphaltenes inside the tubes. At steady state the temperature of the liquid asphaltenes was around 230°C. Then, by pressurizing the vessel up to around 5 psig, asphaltenes flowed and sprayed using hot nitrogen. As described before, nitrogen was heated with an inline heater just before entering the spray configuration. The gas residence time for all of the experiments was fixed to 4 seconds using nitrogen flow. Further, a pressure difference controller (PDC) controlled the pressure inside the tube to be close to atmospheric.

3.4 Asphaltenes char characteristics

Table 3-2-2 shows the proximate and ultimate analysis of chars from asphaltenes obtained at different pyrolysis temperatures. In the table, FC stands for fixed carbon and VM for volatile matters. The moisture content for all the chars was almost zero. Proximate analysis data are also summarized in figure 3-4. According to the results, apparently chars obtained at lower temperatures contain less volatile matters and more fixed carbon. Also, as

pyrolysis temperature increases from 800 to 1000°C, the rate of the rejection of hydrogen from char increases.

Table 3-2 - Proximate and ultimate analysis of asphaltenes chars

Pyrolysis Temp.	Proximate analysis			Ultimate Analysis					H/C ^a
	FC	VM	ASH	C	H	N	S	O*	
Asphaltenes	61.72	37.88	0.52	82.70	7.42	1.15	7.96	0.77	1.08
800	79.63	19.67	0.70	83.84	3.72	1.60	6.79	3.97	0.53
1000	77.70	19.36	2.94	83.41	4.18	1.85	8.03	2.32	0.60
1100	54.02	43.25	2.73	82.06	6.87	1.36	7.44	2.27	1.00
1200	56.47	42.17	1.36	58.77	1.01	0.71	1.63	37.89	0.21
1400	60.82	37.32	1.86	86.15	5.20	1.23	6.67	0.74	0.72

* By difference

^a Molar ratio

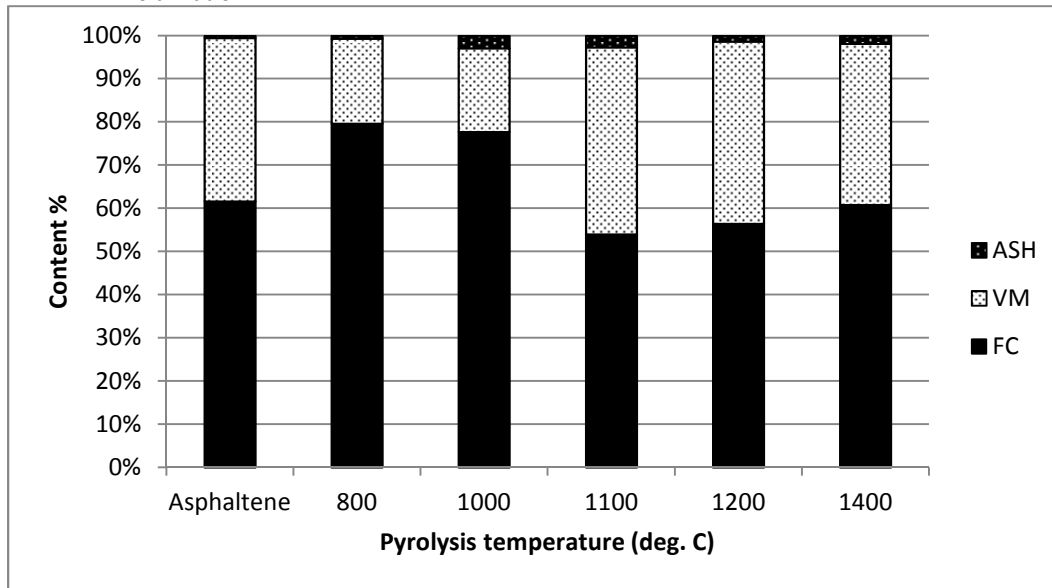


Figure 3-4 - Proximate analysis for asphaltene chars

The high volatile matter content in chars at high temperature is surprising since usually by increasing the pyrolysis temperature, more

volatiles escape from the particles. Considering the design of the apparatus this much volatile matter can be attributed to the heterogeneous condensation of volatiles on the particles. As a matter of fact, in the absence of oxygen in the system, volatile matters did not burn and remained in the system. Further, since the gas (which carries char particles) was cooled down in the collection probe using air to less than 100°C, it is postulated that heterogeneous condensation of volatiles took place in that part. As a matter of fact, heterogeneous condensation is condensation of volatiles on the surface of char particles. This phenomenon enlarges the fine particles. To confirm this hypothesis larger char particles (i.e. particles with size of around 1mm) selected from the same sample (i.e. 1400°C char) to be examined again for volatile matter content. The new results showed that the volatile content of larger particles was 37.32%, which is higher than the volatile matters of the finer particles (i.e. 20.97%).

3.4.1 Char Reactivity

3.4.1.1 Effect of temperature

Reactivity of chars from asphaltenes obtained at different pyrolysis temperatures was measured using air at 475°C with TGA. Figure 3-5 shows the TGA curves for asphaltenes chars reacting with air at 475°C.

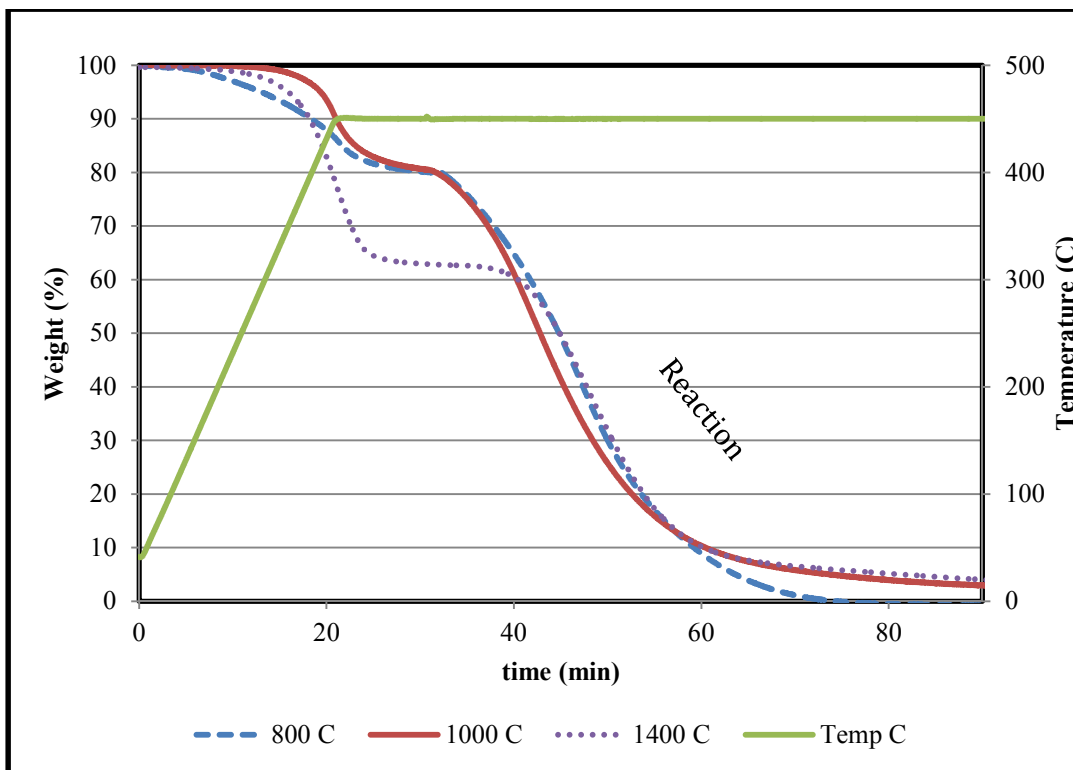


Figure 3-5 - Asphaltenes chars reactivities with air at 475°C

The char samples were heated up to 475 °C under N₂ atmosphere to remove any moisture and volatiles. Once the weight loss was stabilized, the gas was switched to air and remained at isothermal condition (i.e. 475°C) until the end of the reaction.

The slope of TGA curves shows the reactivity of chars with air. It shows that pyrolysis temperature does not have significant effect on the reactivity of chars from asphaltenes since the slopes are all the same, whereas a higher pyrolysis temperature results in a higher degree of carbonisation and lower char reactivity. On the other hand, the chars

obtained at higher pyrolysis temperature interestingly contain more volatile matters. This was attributed to the heterogeneous condensation that was explained in section 3.4

3.4.1.2 Effect of residence time

Figure 3-6 shows the TGA curves for char samples obtained at 1400°C with different residence times of 5, 7.5, and 10 seconds. The residence time was adjusted using N₂ flow rate inside the drop tube.

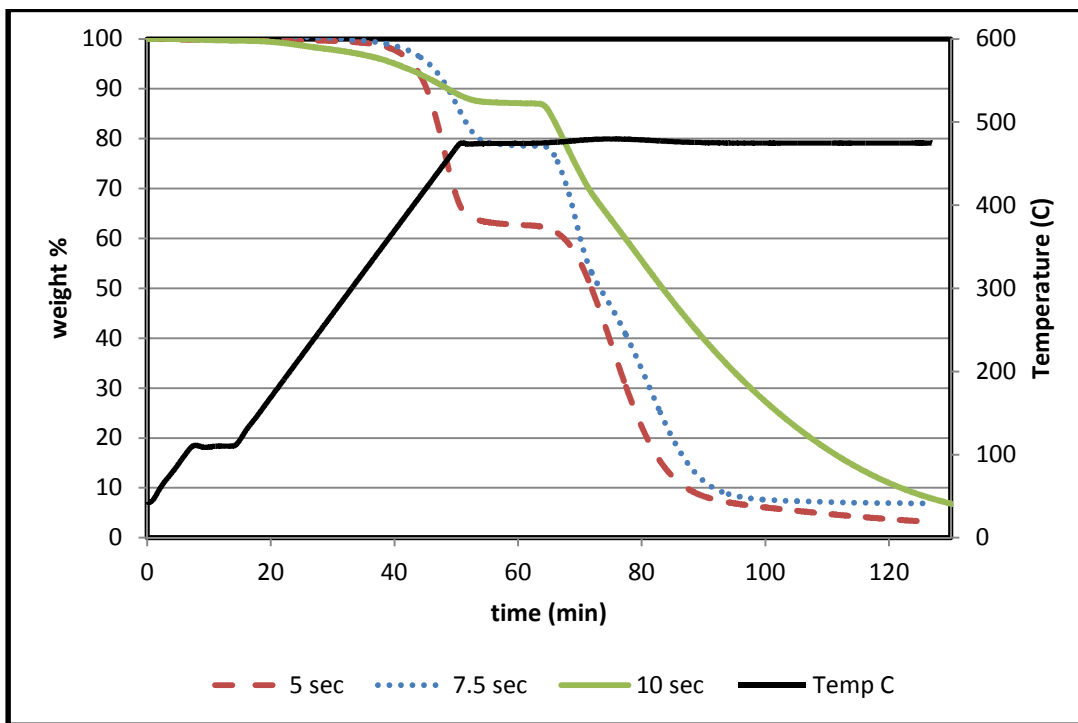


Figure 3-6- Effect of pyrolysis residence time on asphaltene chars reactivity (with air at 475°C)

According to Figure 3-6, chars with higher residence time have less volatiles due to being exposed to high pyrolysis temperature for longer periods. The figure also shows that chars with longer residence time represent less reactivity with air. It can be explained by the fact that heat treatment for those chars lasted longer. Therefore, those chars reached a higher degree of carbonization. Generally, pyrolysis and heat treatment cause severe modifications to the surface of the materials. At early stages, oxygen and hydrogen atoms escape from the sample. The second stage is conversion of mineral matter to the metal oxides and the last stage is thermal annealing during which carbon edges are lost and the char structure becomes more organized and closer to graphite (i.e. graphitization). Since oxygen, hydrogen, minerals and carbon edges are all active sites, heat treatment decreases the reactivity of the char by removing these factors.

3.4.2 Morphological analysis of asphaltenes chars

Figure 3-7 shows SEM images of char particles from asphaltenes obtained at different pyrolysis temperatures from 800 to 1400°C. According to the images, chars obtained at lower temperatures (i.e. up to 1100°C) are compact with solid and uniform surface and rather sharp edges. At 1400 ° C, fine materials are formed on the surface of larger particles. The formation of fine materials could be attributed to the heterogeneous condensation at the cooling section in the collection probe.

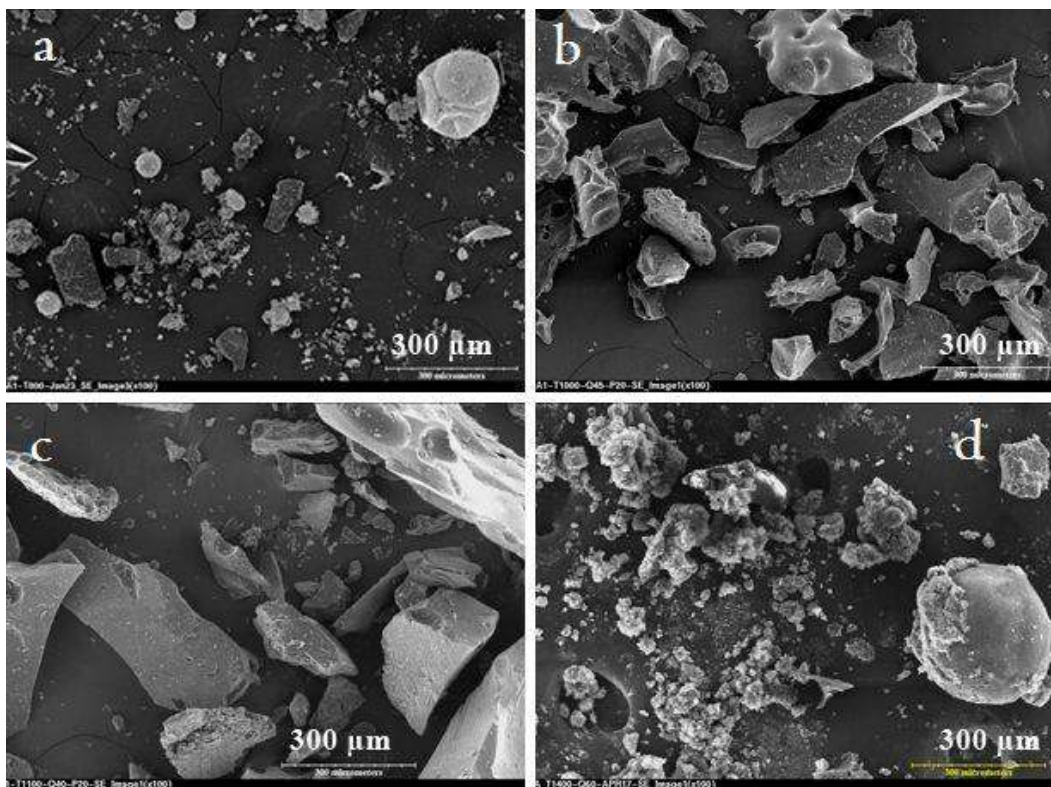


Figure 3-7 - SEM images of chars from asphaltenes at (a) 800°C (b) 1000°C (c) 1100°C and (d) 1400°C

Figure 3-8 shows a closer look at the asphaltenes chars at temperatures below 1400°C. As mentioned before, at temperatures in the range of 800 to 1100°C the chars are compact and spongy. The chars surface is almost non-porous which is in accordance with the observations of Fouga *et al.* (23). They also reported very low porosity for the chars from asphaltite, which is very similar to asphaltenes. The surface area of asphaltenes char in this study obtained at 1300°C measured using Autosorb iQ by nitrogen adsorption at 78K. The results interpreted using multipoint BET. The BET surface area of asphaltenes char at 1300°C was 0.060 m²/gr.

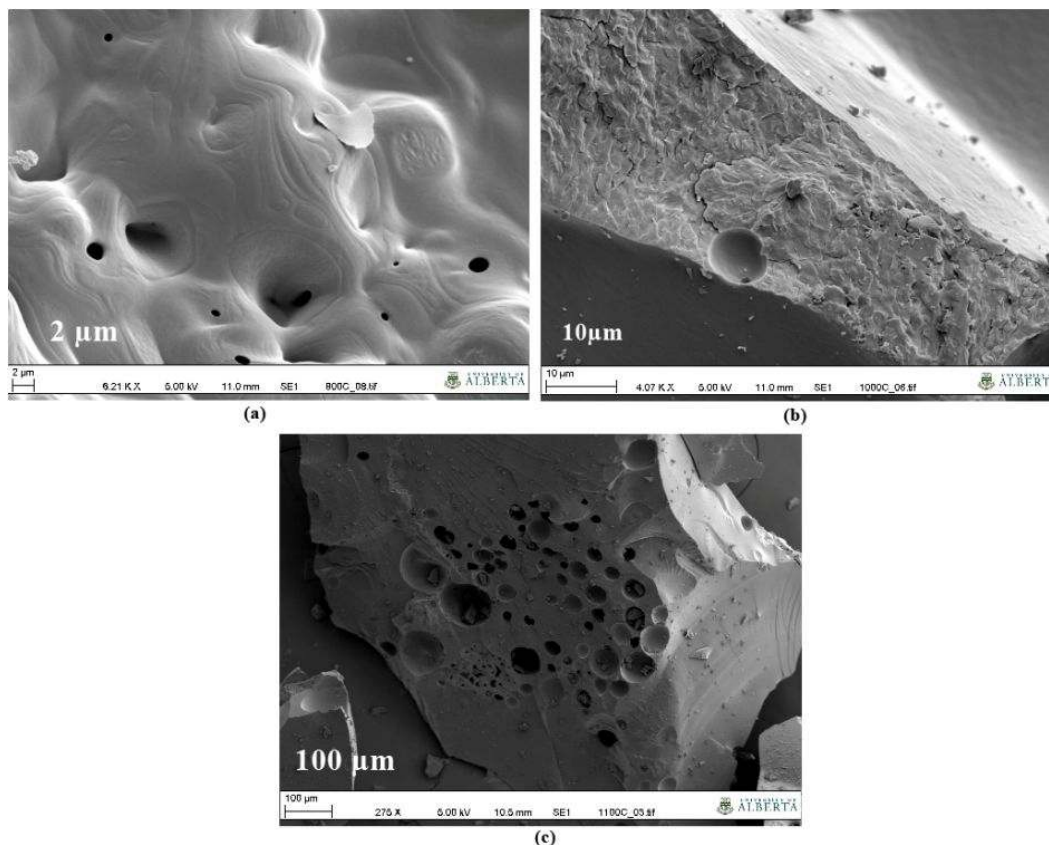


Figure 3-8 - Asphaltene chars at (a) 800°C, (b) 1000°C and (c) 1100°C

Figure 3-9 shows the closer look of asphaltene char particles obtained at 1400 °C. Unlike the chars obtained at lower temperatures, 1400 °C chars are covered with very fine particles, which are supposed to be formed by heterogeneous condensation as described in section 3.4. The formation of very fine particles on the surface of particles is reported in another study by Latva *et al.* (26) shown in Figure 3-10 which is very similar to the SEM results of this work. The authors concluded that ultrafine particles are as a result of heterogeneous condensation happened in their experiments.

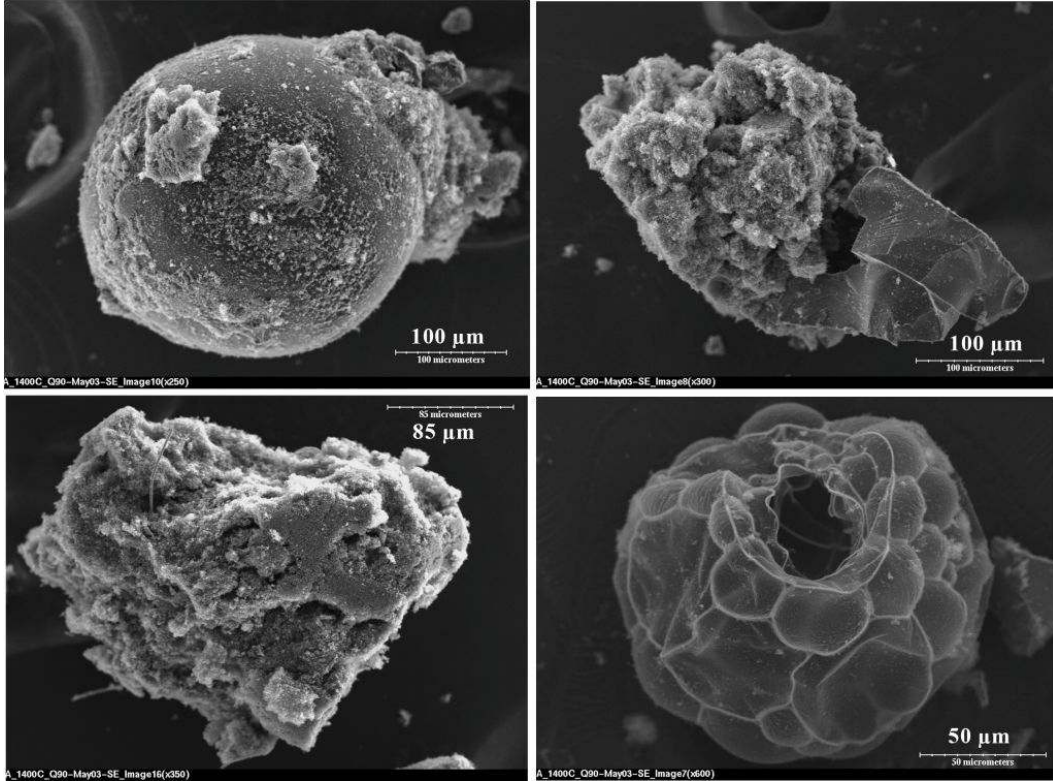


Figure 3-9 - Asphaltenes char particles obtained at 1400°C

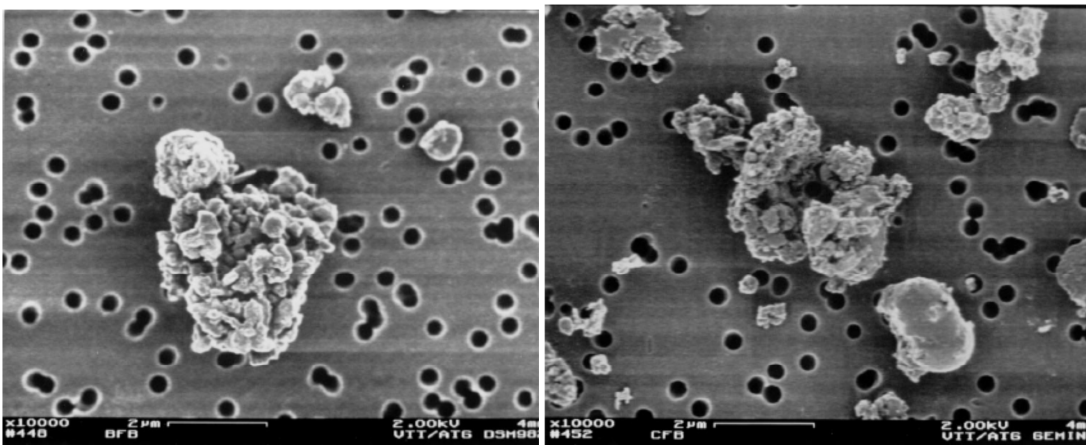


Figure 3-10 - HR-SEM micrographs from waste wood firing. Larger particles covered with ultrafine particles observed by Latva *et al.* (26)

3.4.3 Particle size distribution

Figure 3-11 illustrates the particle size distribution (PSD) curves of asphaltene chars that were obtained at various pyrolysis temperatures. Each PSD shows three curves with different colors that are for three measurements done using Malvern Mastersizer 2000. Since char particles were hydrophobic and could not be dispersed in water, they were dispersed in isopropanol. Also, Figure 3-12 summarizes the particle size distributions results.

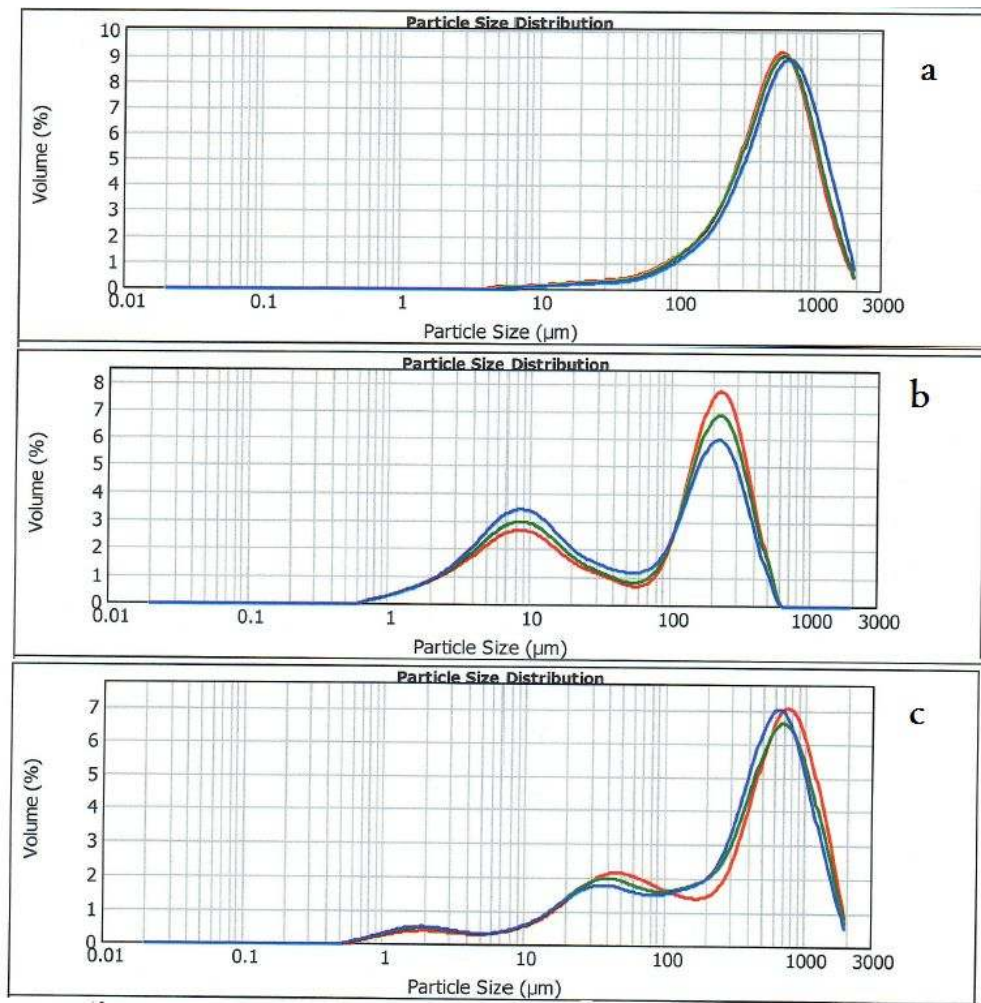


Figure 3-11 - Particle size distribution for asphaltene chars obtained at (a) 1100 °C (b) 1200 °C (c) 1400 °C

As can be seen in Figure 3-12, the particle size increases with increasing temperature. This can be attributed to the heterogeneous condensation of volatile matters in the collection probe discussed in section 3.4. Although the spray condition was tried to be kept the same at all the experiments, the change in the spraying gas flow and pressure may have affected the particle size distribution.

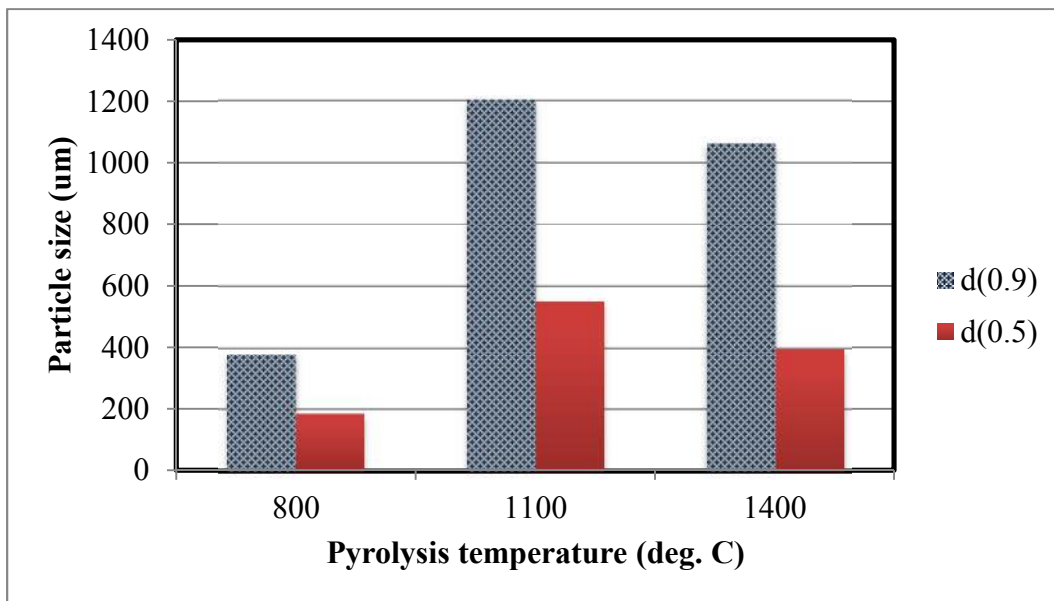


Figure 3-12 - Particle size distribution for asphaltene chars

3.5 Characteristics of slurry chars

3.5.1 Proximate and ultimate analyses

Table 3-3 shows the proximate and ultimate analysis of chars from 10% Genesee coal (GC)-asphaltene slurry obtained at different pyrolysis temperatures. FC stands for fixed carbon, VM for volatile matters. The

moisture content was almost zero. Proximate analysis data are also summarized in Figure 3-13. According to the data, fixed carbon content increases with increasing the pyrolysis temperature. Decreasing the sulfur content of the samples indicates that by increasing the temperature, more sulfuric content escape from the char residue. The H/C ratio, which is an indicator of char reactivity, decreases because of the hydrogen rejection from char at higher temperatures. Therefore, it is expected that slurry chars obtained at higher pyrolysis temperatures have lower reactivities. The results also reveal that slurry chars prepared at 1200 and 1300 °C are similar while there is a change in the characteristics of chars prepared at 1400°C. This indicates the evolution of a different mechanism that determines the char characteristics at temperatures higher than 1300 °C. This assumption will be confirmed in terms of reactivity further in section 3.5.3.

Table 3-3 - Proximate and ultimate analysis of slurry chars

Pyrolysis Temp.	Proximate Analysis			Ultimate Analysis					H/C ^a
	FC	VM	ASH	C	H	N	S	O*	
1200	70.59	21.68	7.73	86.13	2.87	1.09	4.93	4.98	0.40
1300	76.74	18.33	4.94	87.52	2.94	1.05	4.91	3.58	0.40
1400	84.78	10.78	4.44	92.61	1.54	0.60	2.56	2.70	0.20
GC_1400	68.25	2.98	21.73	70.45	0.54	0.68	0.21	28.12	0.09

* By difference

^a Molar ratio

Moreover, by comparing the characteristics of the slurry chars with asphaltenes char, it can be seen that slurry chars have less volatile and more fixed carbon than the asphaltenes chars at the same temperatures. Furthermore, H/C ratio is also higher in asphaltenes chars, which indicates a higher reactivity.

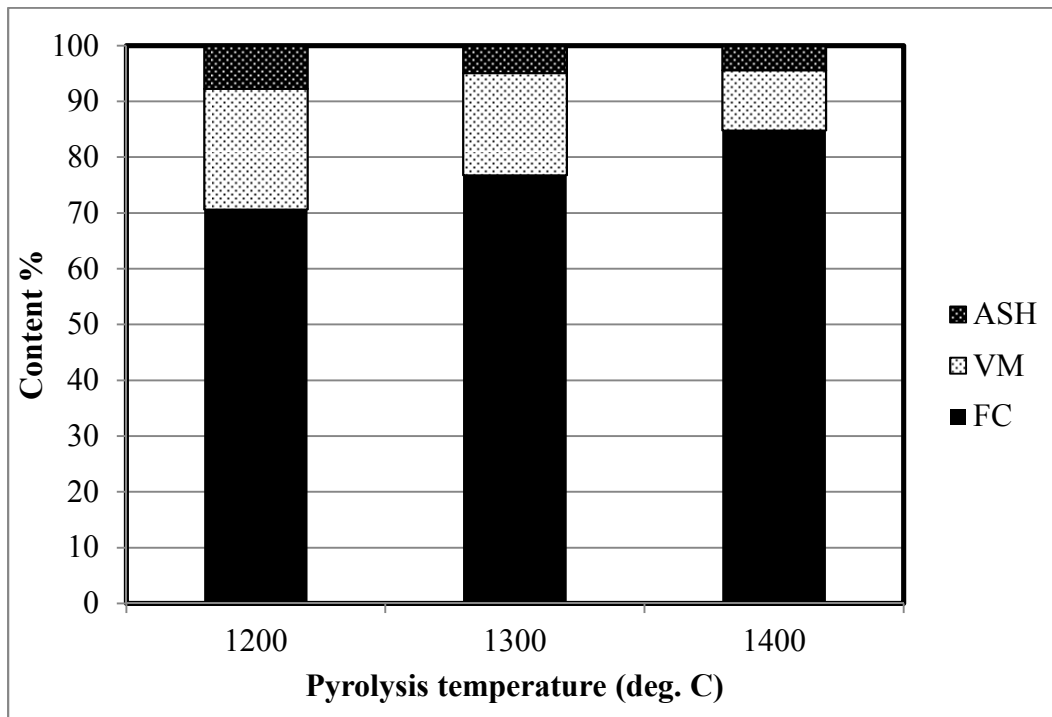


Figure 3-13 - Proximate analysis of slurry chars

3.5.2 Morphology analysis of slurry chars

SEM images of chars obtained from pyrolysis of 10% GC coal in asphaltenes slurry at 1200, 1300 and 1400 °C is shown in Figure 3-14. Obvious similarity between the chars indicates that the pyrolysis temperature does not affect the shape of chars. The slurry chars are also very

similar to the asphaltenes char obtained at 1400 °C. In both cases, the char particles are covered with very fine particles. Figure 3-15 provides a clearer picture of the slurry char particles obtained at 1400 °C. The surface area of slurry char prepared at 1400 °C measured using Autosorb iQ by nitrogen adsorption at 78K. The results interpreted using multipoint BET. The BET surface area of asphaltenes char at 1400°C was 0.007 m²/gr, which is smaller than the surface area of asphaltenes char reported in section 3.4.2.

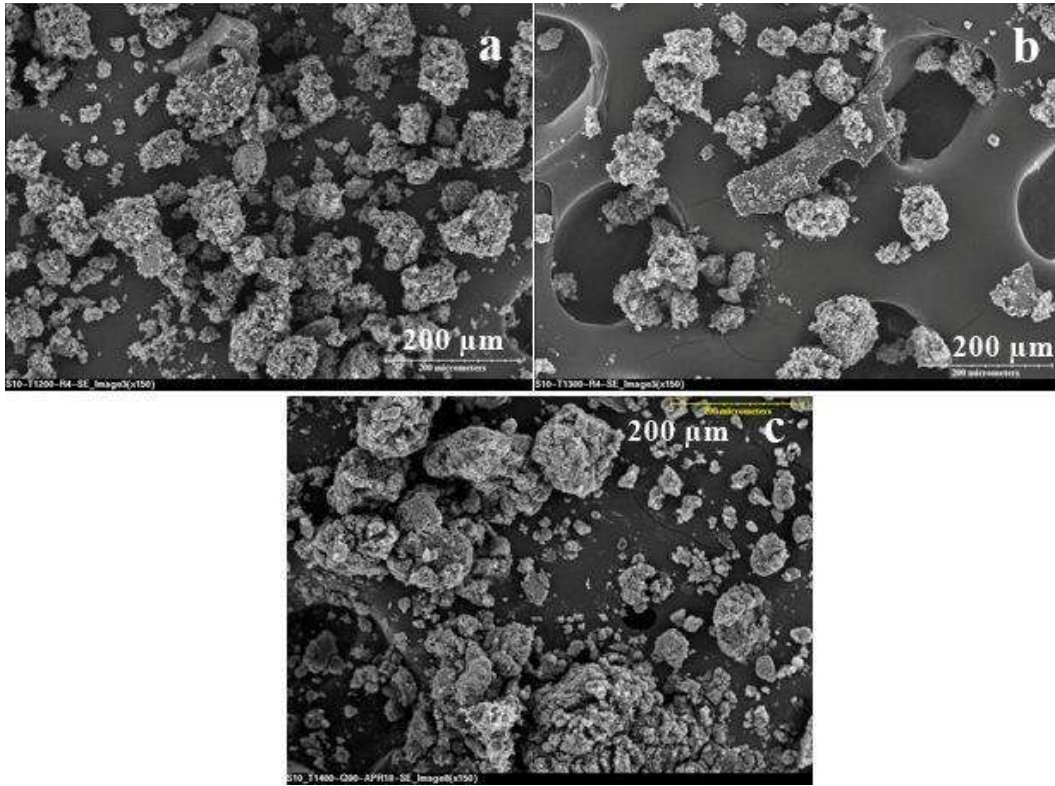


Figure 3-14 - SEM images of chars from coal-asphaltene slurry at (a) 1200°C (b) 1300°C and (c) 1400°C with the same residence time of 4 seconds

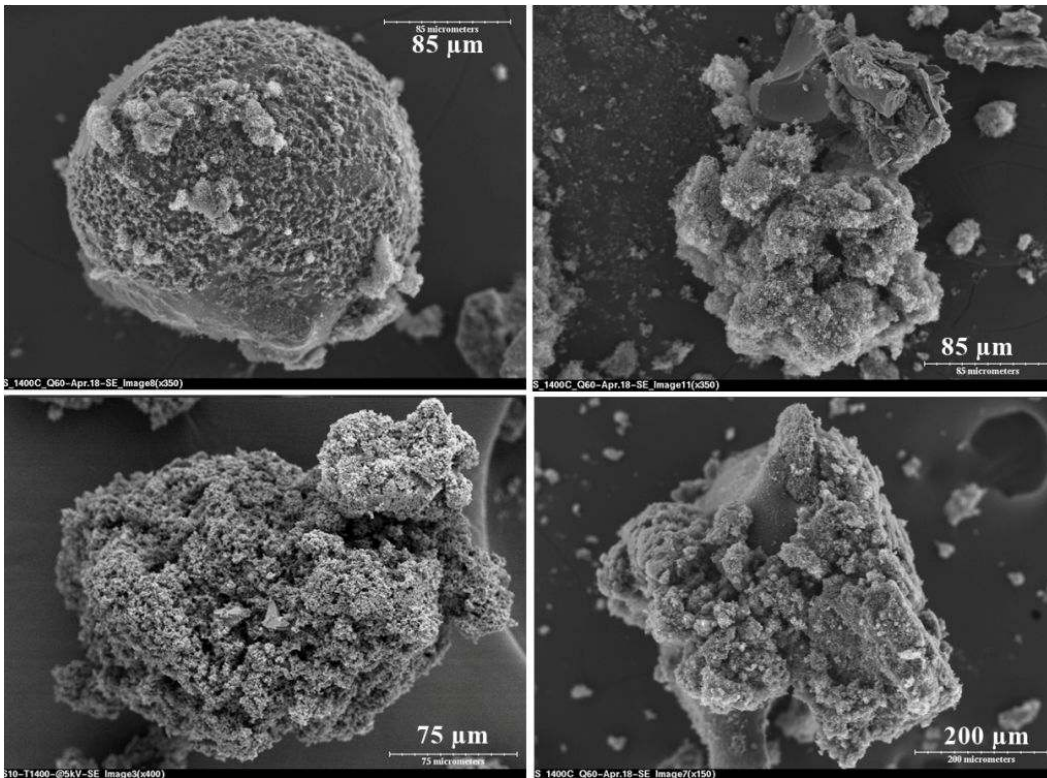


Figure 3-15 - Slurry chars obtained at 1400 °C

3.5.3 Reactivity of slurry chars

Figure 3-16 illustrates the typical TGA curve for the reaction of the coal- asphaltenes slurry char with oxygen at 475 °C. The TGA procedures were described in section 3.4.1 for asphaltenes chars. The slope of the TGA curve shows the reactivity of the slurry char with oxygen at the desired temperature. According to the TGA curves provided in Figure 3-17, the slurry chars react with air with two mechanisms because two different slopes appear in the TGA graph. It can be postulated that the coal part and asphaltenes part in the slurry char separately involve in the reaction and do not interfere with each other. For example, the first slope can be attributed to

the reaction of the asphaltenes part and the second slope to the coal part. This postulation will be discussed more in the next chapter of this thesis. Therefore, these two sections of the TGA curve with different slopes will be called zone I and zone II in further sections of the thesis.

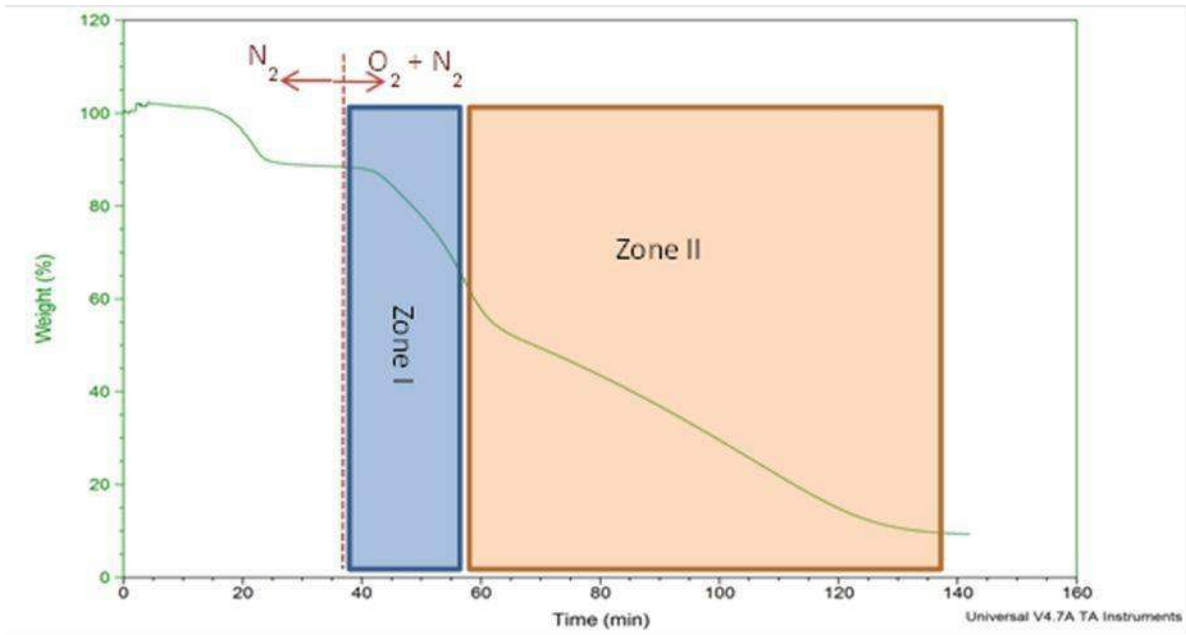


Figure 3-16 - Typical slurry char TGA curve for reaction with O_2

Figure 3-177 shows the TGA curves regarding the reactivity of GC coal in asphaltenes slurry chars at 475°C with air. The chars were obtained at 1200, 1300 and 1400°C.

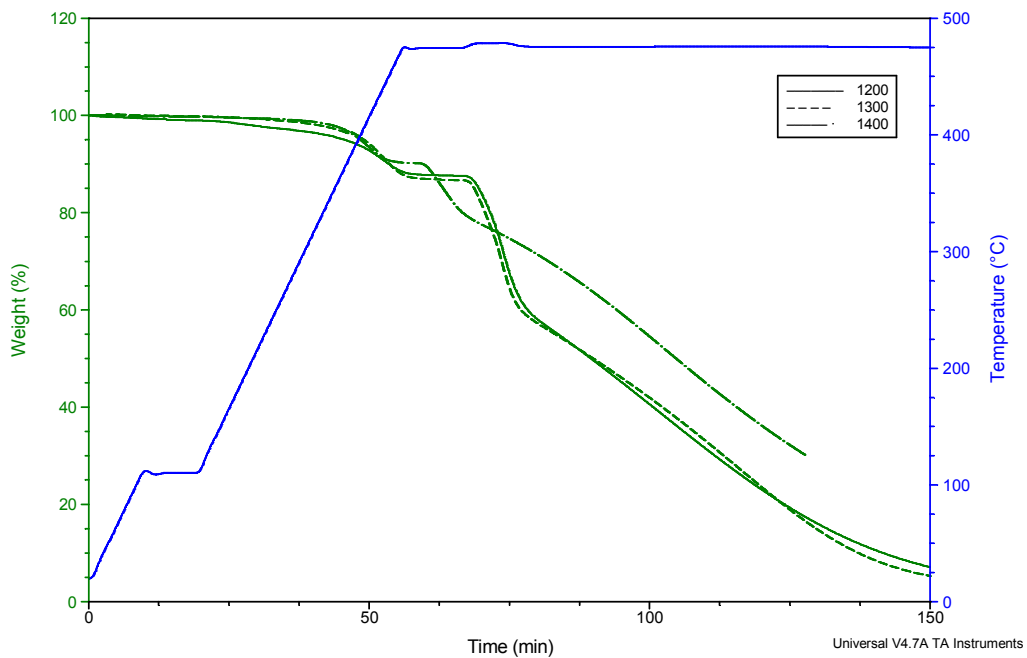


Figure 3-17 - Reactivity of slurry chars with air at 475°C

Figure 3-17 3-16 shows that chars obtained at 1200 and 1300°C exhibit similar reactivities since their slopes at either zones (i.e. zone I and II) are very close to each other. This further confirms the similarity of slurry chars obtained at 1200 and 1300°C discussed before in section 3.5.1.

Figure 3-18 shows TGA reactivity curves of chars from asphaltenes (non-slurry) and coal-asphaltenes slurry both obtained at 1400°C. The figure shows that the char from slurry contains less volatile compared to asphaltenes char. Slurry char volatile matter is about 10% and does not change significantly with residence time. On the other hand, asphaltenes char

has 38% volatiles at 5 seconds residence time and it decreases to 22% at 7.5 seconds residence time. In other words, the difference between volatiles in slurry and asphaltene chars is about 8% for the chars obtained at 7.5 residence time while it is about 28% for the chars obtained at 5-second residence time.

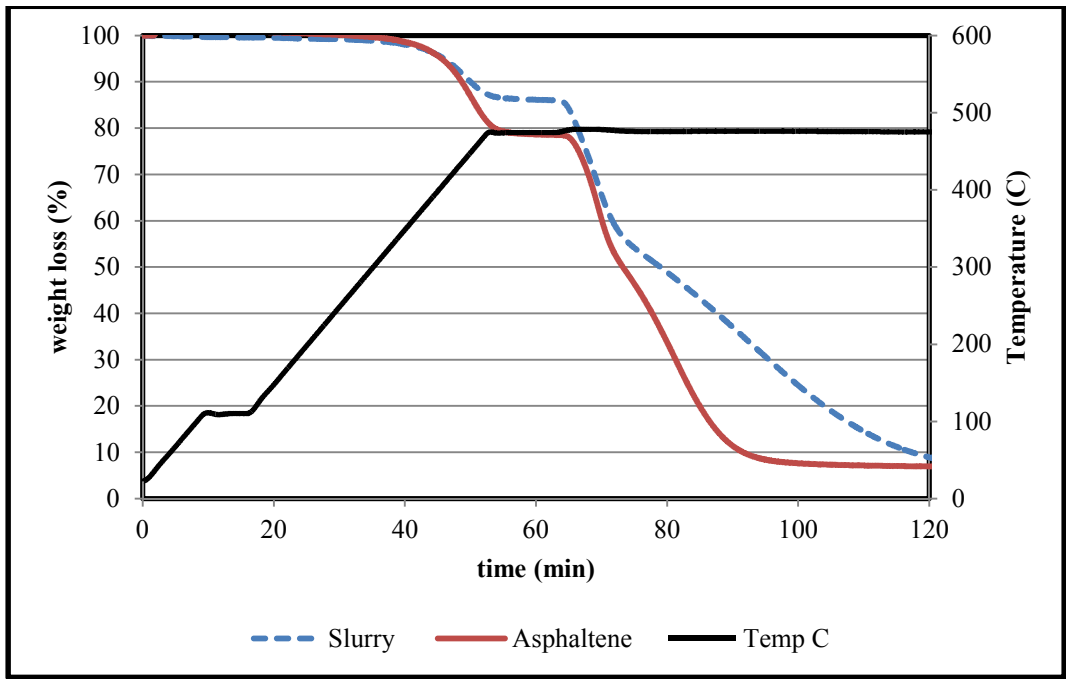
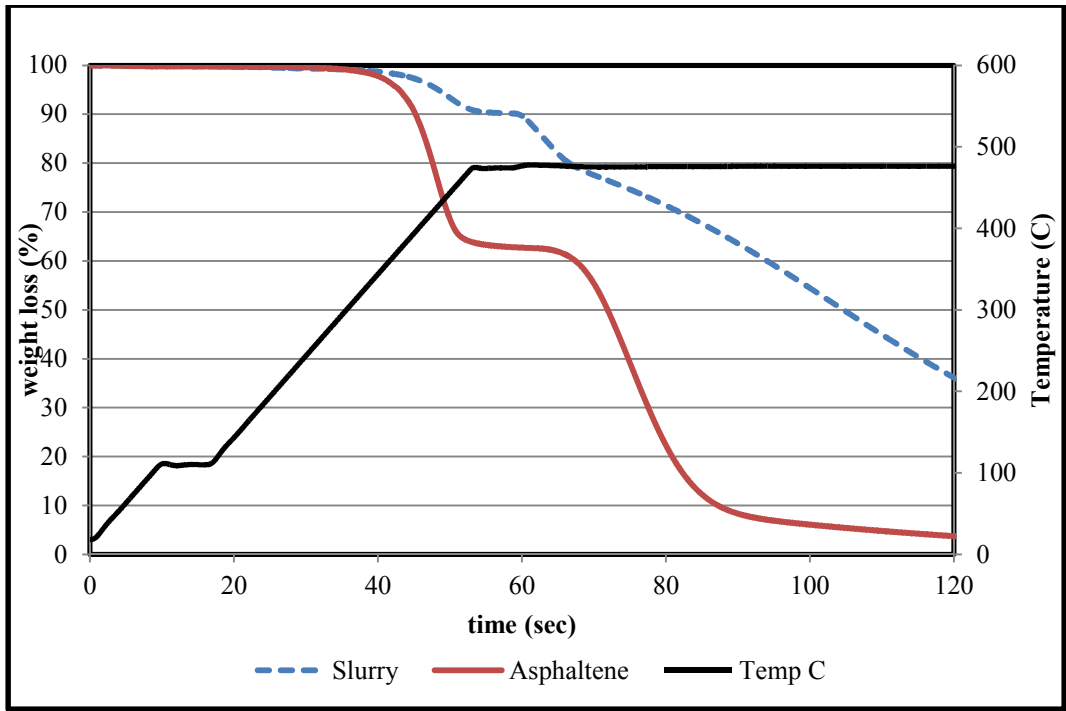


Figure 3-18 - TGA curves for slurry and non-slurry chars at (a) 5 sec and (b) 7.5 sec residence time

The reactivity curves of the slurry chars also show that they burn with two different mechanisms since the curves have two slopes. Since the slope of the slurry char in the first zone is closer to the slope of asphaltenes char, it can be explained that in slurry char, first the asphaltenes part and then the coal part burn. According to the slopes of asphaltenes and slurry chars in Figure 3-18, the reactivity of slurry chars are lower. Therefore, it can be concluded that the mixing of coal and asphaltenes produces chars with lower reactivity and since the different parts of the slurry char react separately there is no advantage in making slurry of these two materials. The difference between slurry and asphaltenes char increases with increasing the residence times.

3.5.4 Particle size distribution

Figure 3-11 illustrates the particle size distribution (PSD) curves of coal-asphaltenes slurry chars that were obtained at various pyrolysis temperatures. Each PSD shows three curves with different colors that are for three measurements done using Malvern Mastersizer 2000. Since char particles were hydrophobic and could not be dispersed in water, they were dispersed in isopropanol. Also, Figure 3-12 summarizes the particle size distribution results.

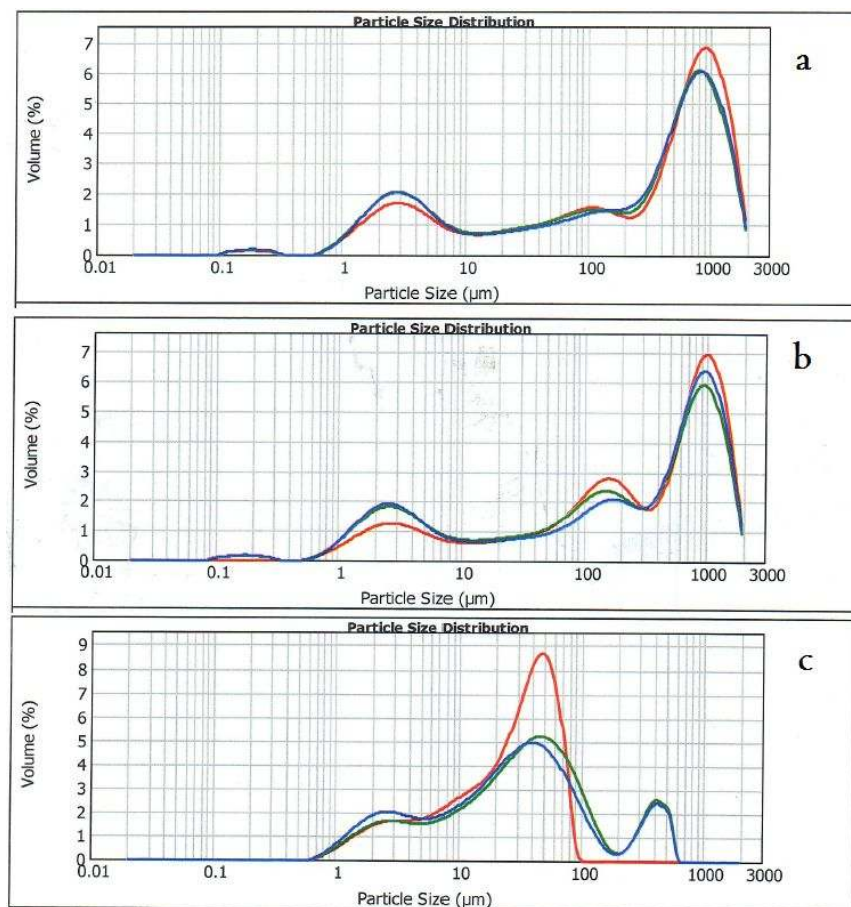


Figure 3-19 - Particle size distribution for slurry chars obtained at (a) 1200 °C (b) 1300 °C (c) 1400 °C

As can be seen in Figure 3-20, the general trend is the reduction of particle sizes by increasing the temperature. It should be mentioned that although the spray condition including the spraying gas flow rate and pressure was the same for all the experiments, the small discrepancies in the spray configuration may affect the particle sizes. Also, due to non-uniformity of a slurry char that consists of solid coal particles as well as liquid asphaltene, the fragmentation of the slurry char particles is more likely.

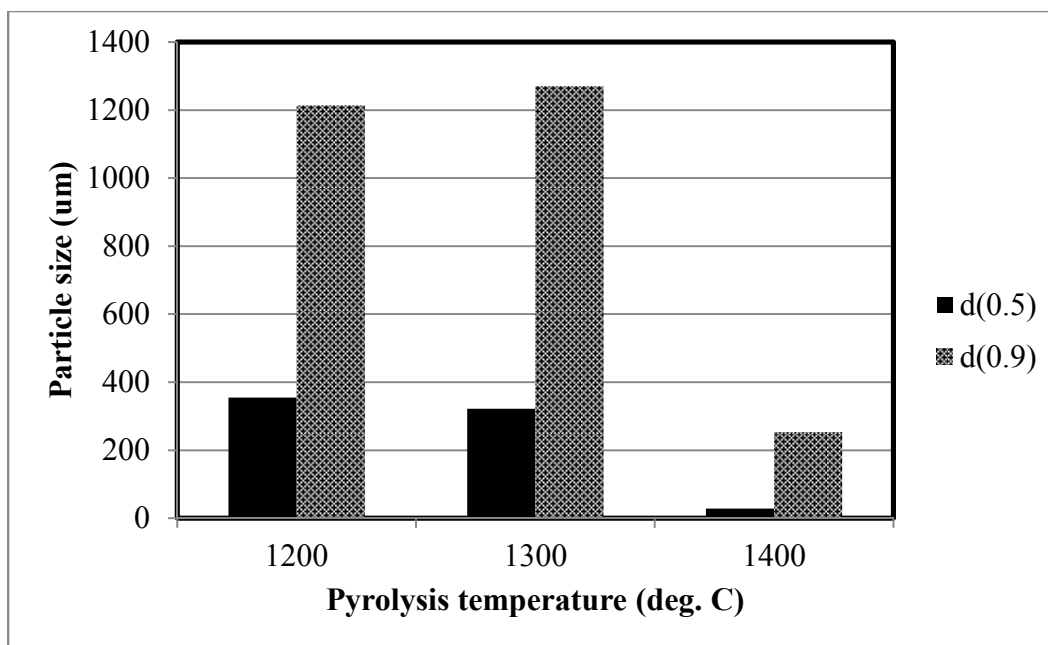


Figure 3-20 - Particle size distribution of slurry chars at different pyrolysis temperatures

3.6 Chapter findings and conclusion

The characteristics of chars from asphaltenes and chars from the slurry of Genesee coal (GC) in asphaltenes were studied in this chapter. The chars obtained from an atmospheric entrained flow drop tube at various high temperatures from 800 to 1400 °C. Char proximate analysis showed that the volatile content of asphaltenes chars obtained at higher pyrolysis temperatures were high and it can be due to the heterogeneous condensation of volatile matters on the char surface in the collection probe, which is air cooled.

TGA experiments with air showed that pyrolysis temperature does not have significant effect on asphaltene char reactivity. On the other hand, increasing the pyrolysis residence time decreased the char reactivity and volatile content.

Moreover, according to the SEM analysis, asphaltene chars that obtained at 1400 °C, were covered with very fine particles which is assumed to be attributed to the heterogeneous condensation. Also, the porosity of the char particles were very low. The characteristics of slurry chars obtained at 1200 and 1300°C were close to each other while it was different than 1400 °C one. It can be concluded that pyrolysis temperature higher than 1400 °C has more effect on the char characteristic than the lower pyrolysis temperatures.

The main finding of this chapter was comparison between the slurry and asphaltene chars. It is found that the slurry char reacts with O₂ with two mechanisms. The kinetic of the two mechanisms will be studied in the next chapter. Also, it is found that overall reactivity of the slurry char is much lower than the reactivity of asphaltene char.

CHAPTER 4

Kinetics of the reactions of asphaltenes and slurry chars with O₂

This chapter discusses the derivation of intrinsic reaction kinetics of asphaltenes chars and coal-asphaltene chars with O₂ from the experimental data provided in the previous chapter.

4.1 The feedstock

A thermogravimetric analyzer (TGA) was used to measure the reactivity of asphaltene char obtained at 1400°C and slurry char obtained at 1300°C from the atmospheric entrained flow drop tube. The feedstock for

asphaltenes char was Athabasca asphaltenes from Nexen's deasphalting plant in Long Lake in Northern Alberta. The slurry char was produced by adding 10% Genesee coal (GC) into the Athabasca asphaltenes. The characteristics of these chars along with ultimate and proximate analyses were presented in the previous chapter. These chars were grounded using a mortar and particle size of pulverized chars was measured with Malvern Mastersizer 2000. The $d(50)$ of the particles was measured to be 40 μm .

4.2 Char preparation

The experimental procedure for char preparation was described in section 3.1.

4.3 TGA experiments

The reactions of char with oxygen were conducted using a TGA (TA instruments Q600, Figure 4-11). The TGA consists of a horizontal balance beam. The beam also holds the sample pan. A thermocouple is in contact with the sample pan directly. A very thin layer of char sample (ca. 2 mg) was spread on alumina pan. The temperature profile starts heating up to the reaction temperature with the rate of 20°C/min under ultra-pure N₂ atmosphere. It remained under N₂ atmosphere at the desired temperature for about 20 min or until the weight change was less than 1%. After the weight percent reached a plateau, it switched to the mixture of N₂ and O₂.

The weight loss was recorded with time and temperature. Because the thermocouples are directly connected to the sample pan in highly exothermic reactions like combustion, it gives more realistic temperature. Also the sensitivity of the balance in order of 0.1 μg using dual beam balance mechanism, according to the manufacturer technical features.

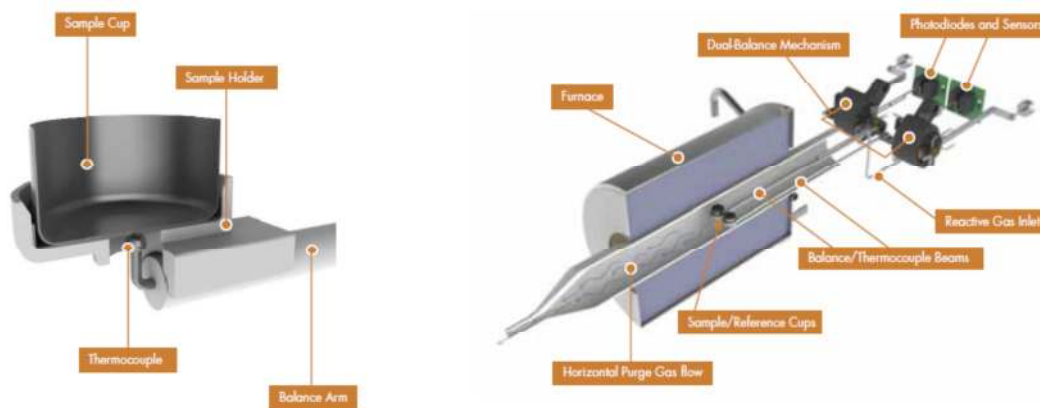


Figure 4-1 - TA instrument Q600 configuration (From TA website)

In order to reduce the effect of mass transfer diffusion, the sample pan was polished from the original 4 mm deep to about 0.5 mm. To ensure that the reactions are chemically controlled, a series of preliminary experiments were conducted with different total gas flow rates and sample weights at the highest temperature used in the kinetic studies. Since the pyrolysis reaction is faster at higher temperatures, if it is chemically controlled at that condition, it should be chemically controlled at lower temperatures as well. According to the preliminary experiments, total flow rate of 300 mL/min and sample weight of about 2 μg were found enough for O_2 reactions to take place

with very little effect of mass transfer resistance. The particle size (i.e. $d(50)$) was $40\mu\text{m}$.

4.4 Treatment of TGA results

The char- O_2 reaction rate calculated based on the TGA data as:

$$r = -\frac{1}{m-m_f} \frac{d(m-m_f)}{dt} \quad (4-1)$$

where m is the mass at time t and m_f is the final weight at the end of reaction.

Considering the reaction conversion as:

$$X = \frac{m_0 - m}{m_0 - m_f} \quad (4-2)$$

where m_0 is the initial weight of the sample recorded by TGA at the beginning of the reaction with O_2 . By substituting the conversion equation into the rate equation we have:

$$r(X) = \frac{1}{1-X} \frac{dX}{dt} \quad (4-3)$$

Thus, the rates of the reactions were calculated based on the slope of the conversion curve versus time. The kinetic rate equation for reaction of char with O_2 assumed to be in the form of power law:

$$r = k_0 e^{-\frac{E_a}{RT}} P_{\text{O}_2}^n \quad (4-4)$$

4.4.1 Slurry char-O₂ reaction

For slurry char obtained at 1300 °C, TGA experiments have been conducted at four temperatures of 425, 450, 475, 500 °C and three different O₂ partial pressures of 505, 1010 and 2020 Pa to obtain kinetic parameters. As explained in section 3.5.3, since in the case of slurry chars the reaction takes place with two mechanisms, the kinetic parameters were separately found for each zone (Figure 3-16).

By changing the equation (4-14) to logarithmic form, we have equation (4-15):

$$\ln r = \ln k_0 - \frac{E}{RT} + n \ln P_{O_2} \quad (4-5)$$

Keeping the oxygen partial pressure constant (i.e. 1% O₂) and doing TGA experiments at 425, 450, 475 and 500°C, the reaction rate were calculated from the slope of conversion profiles using the equation (4-13) in the range of conversions between 5%-35% for the 1st zone and between 45%-90 % for the 2nd zone. Figure 4-2 shows the Arrhenius plots ($\ln r$ vs. $1/T$) for the 1st and the 2nd zones for the reaction of slurry char obtained at 1300°C with oxygen. The linear trend of points for both zones confirms that the chemical control regime prevails and the effect of diffusional mass transfer is negligible. According to the Arrhenius plots in Figure 4-2, the activation energy is determined to be 99.61 kJ/mol for zone I and 143.28 kJ/mol for zone II.

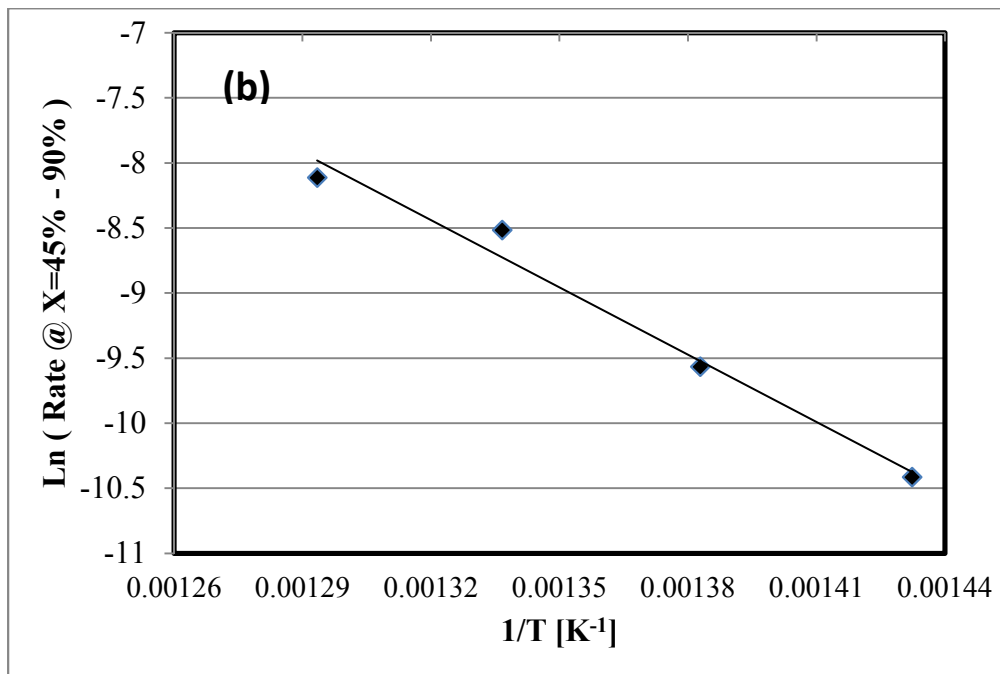
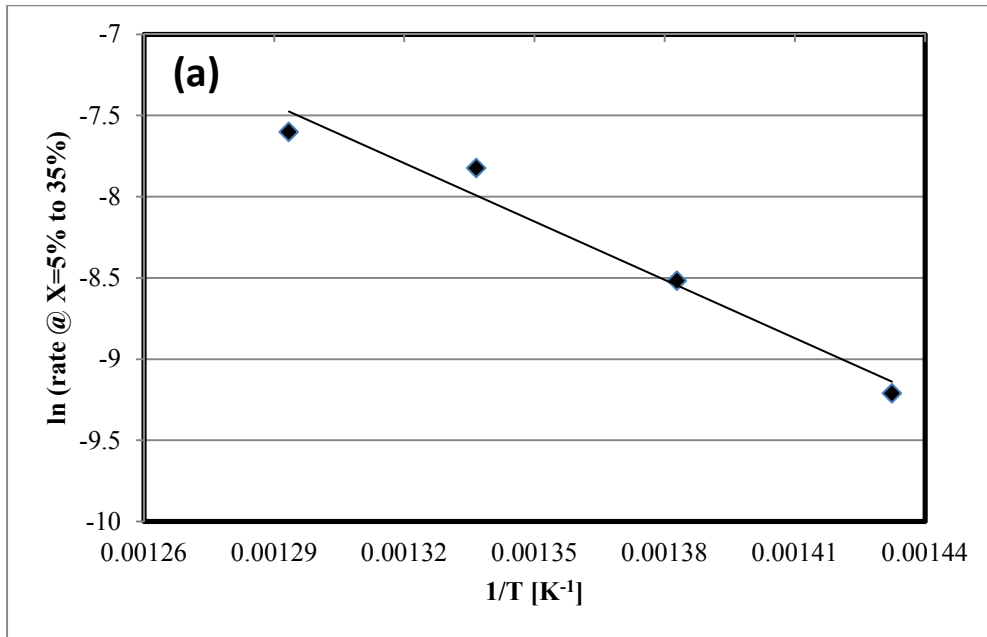


Figure 4-2 - Arhenius plots for reaction of slurry char (obtained at 1300°C) with 1% O₂ in the range of 425-500°C for (a) Zone I and (b) Zone II

Figure 4-3 shows the conversion profiles for char-O₂ reaction at 475°C and with different partial pressures of O₂. Different reaction mechanisms are seen in the conversion profiles since the slope of the profiles are changed around 40% conversion. The order of reaction with respect to partial pressure of oxygen was calculated using equation 4-15. The reaction rates with oxygen measured at different partial pressures of 505, 1010 and 2020 kPa at 475°C. Figure 4-4 illustrates $\ln(\text{rate})$ vs. $\ln(P_{O_2})$ for reaction of slurry char (obtained at 1300°C) with 0.5, 1 and 2 % at 475°C. Again, reaction rates were calculated from the slope of conversion profiles.

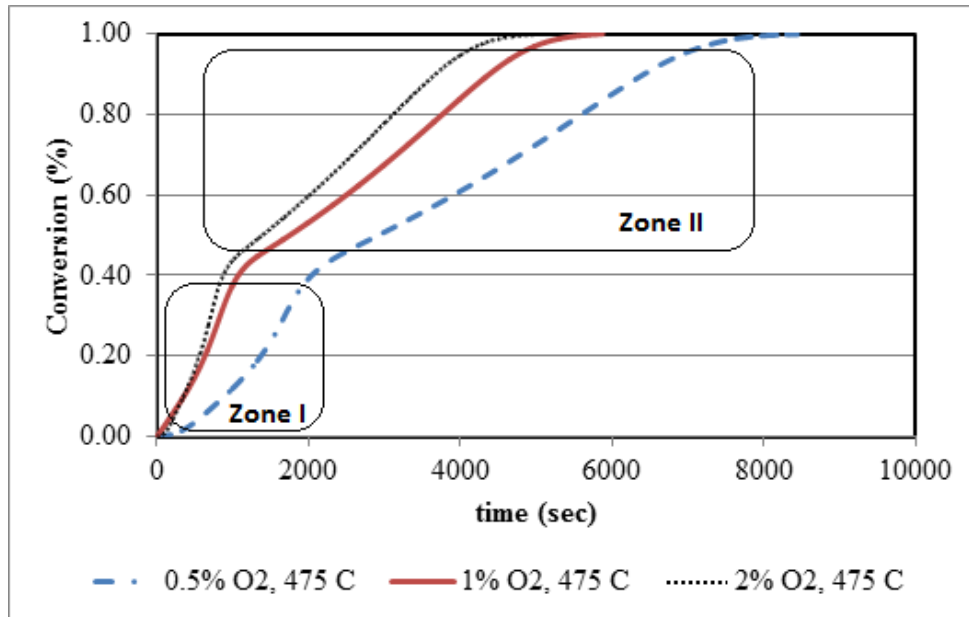


Figure 4-3 - Conversion profiles for slurry char (1300 °C) with O₂ reaction at 475°C and different O₂ partial pressures

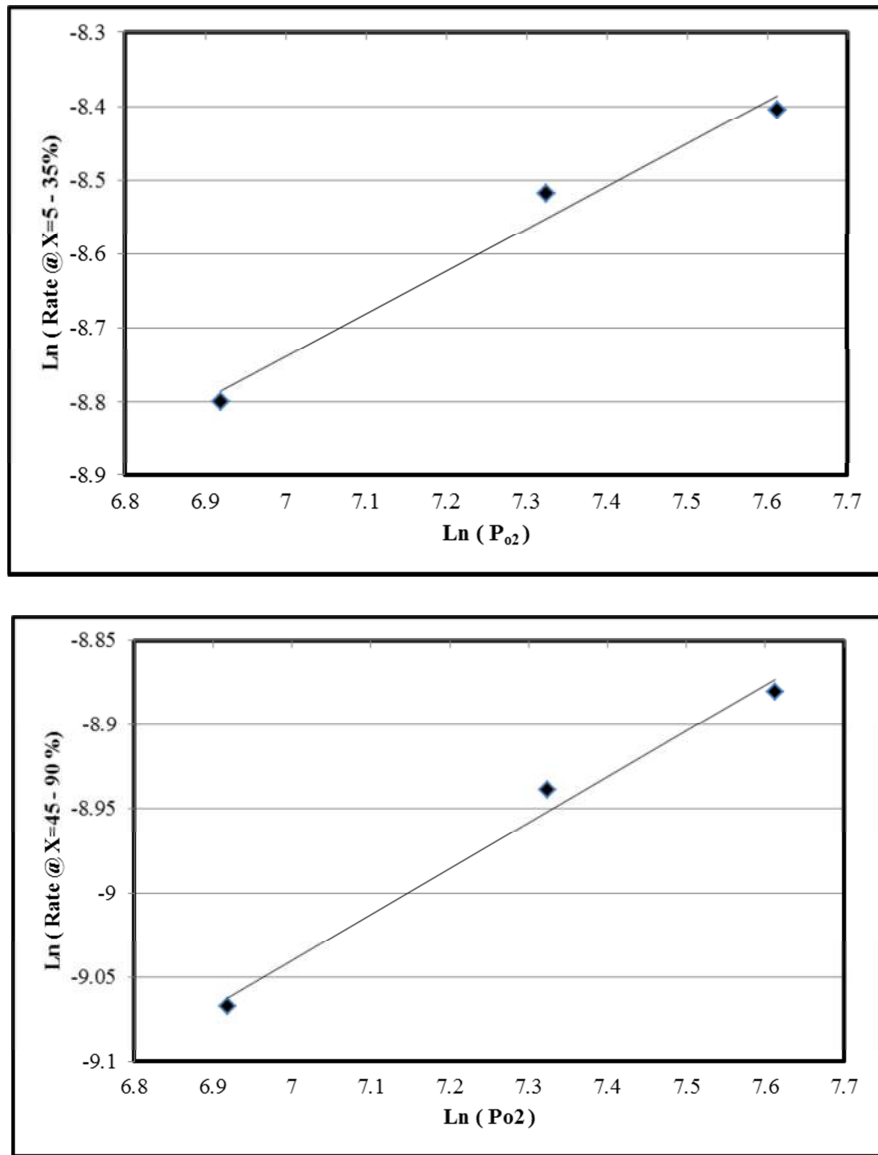


Figure 4-4 - $\ln(\text{rate})$ vs. $\ln(P_{O_2})$ for reaction of slurry char (obtained at 1300°C) with 0.5, 1 and 2 % at 475°C for (a) Zone I and (b) Zone II

According to the equation 4-15, the slope of plots in Figure 4-4 shows the order of reaction with respect to the partial pressure of O_2 . It is calculated

as $n=0.66$ for the 1st zone and $n=0.5$ for the 2nd zone. Therefore, the kinetic reaction rate for slurry char can be summarized as:

$$r = 3.04 \times 10^3 e^{-\frac{99.610 \text{ kJ/mol}}{RT}} P_{O_2}^{0.66} \quad \text{for } X < 40\%$$

$$r = 1.636 \times 10^6 e^{-\frac{143.275 \text{ kJ/mol}}{RT}} P_{O_2}^{0.5} \quad \text{for } X > 40\%$$

The same set of TGA experiments were conducted on slurry char, which obtained at 1400 °C. The experiments carried out at four temperatures of 450, 475, 500 and 550 °C and three oxygen partial pressures of 1011, 1516 and 2022 Pa (1%, 1.5% and 2%O₂ in nitrogen) at 475°C. Figure 4-5 shows the Arrhenius plots for 1400°C slurry char for the 1st and the 2nd zones. Since the 1st zone in this case was in a smaller range of conversion, the rate was calculated from the conversion profile between 5% - 10% for the first zone and between 15% and 90% for the second zone.

According to the experiments, the activation energy for Zone I is calculated as 69.20 kJ/mol and for Zone II as 116.76 kJ/mol. The order of reaction with respect to oxygen partial pressure is calculated as $n=0.58$ for Zone I and $n=0.27$ for Zone II.

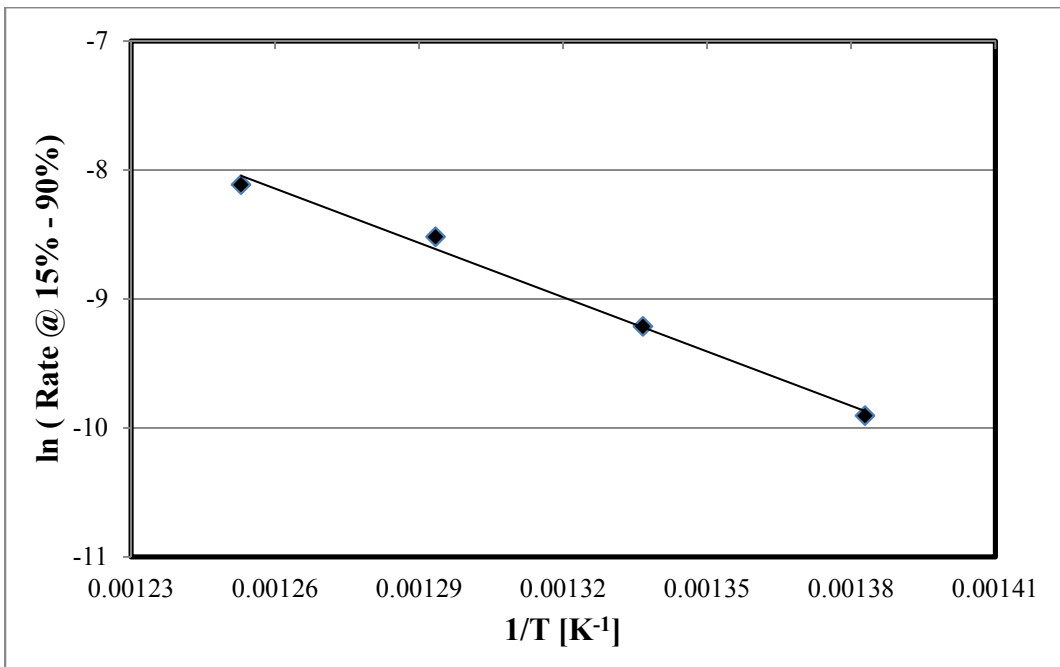
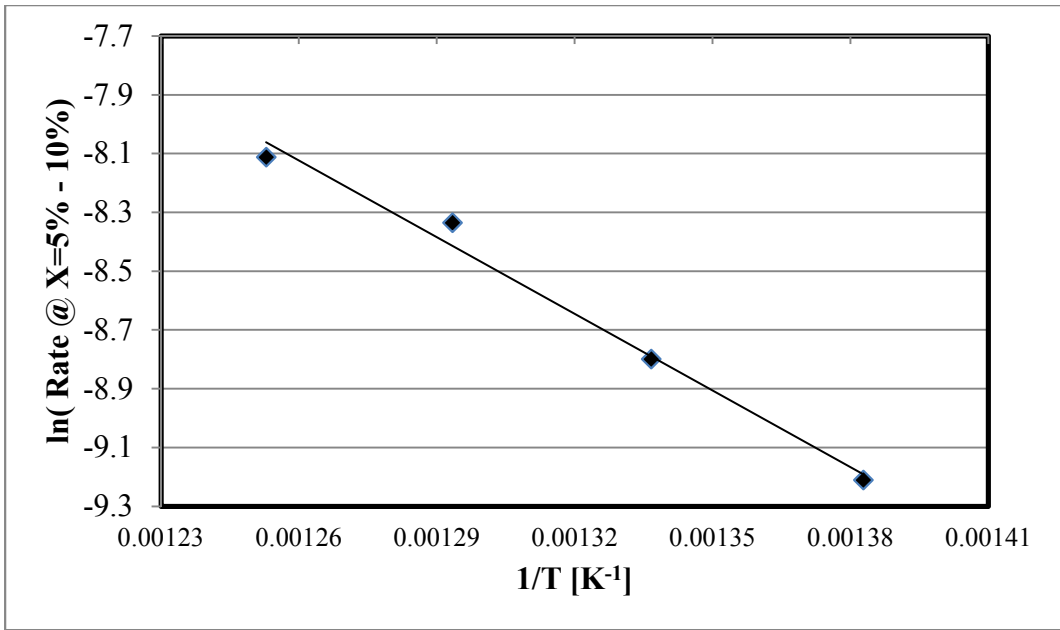


Figure 4-5 - Arhenius plots for slurry chars obtained at 1400 °C (a) Zone I and (b) Zone II

4.4.2 Asphaltenes char-O₂ reaction

Asphaltenes char obtained at 1400 °C was chosen for the kinetic study. TGA experiments with asphaltenes char have been conducted at three temperatures 450, 475, 500 °C and three different O₂ partial pressures of 505, 1010 and 2020 Pa for the purpose of obtaining the kinetic parameters. The procedure for treatment of TGA results is the same as slurry char. The reaction rate was calculated from the slope of conversion profiles, plotted in Figure 4-6, between X=10%-90%. According to the Arrhenius plot (Figure 4-7) for the asphaltenes char, the activation energy was calculated to be 64.76 kJ/mol. The order of the reaction with respect to partial pressure of O₂ was found to be 0.45.

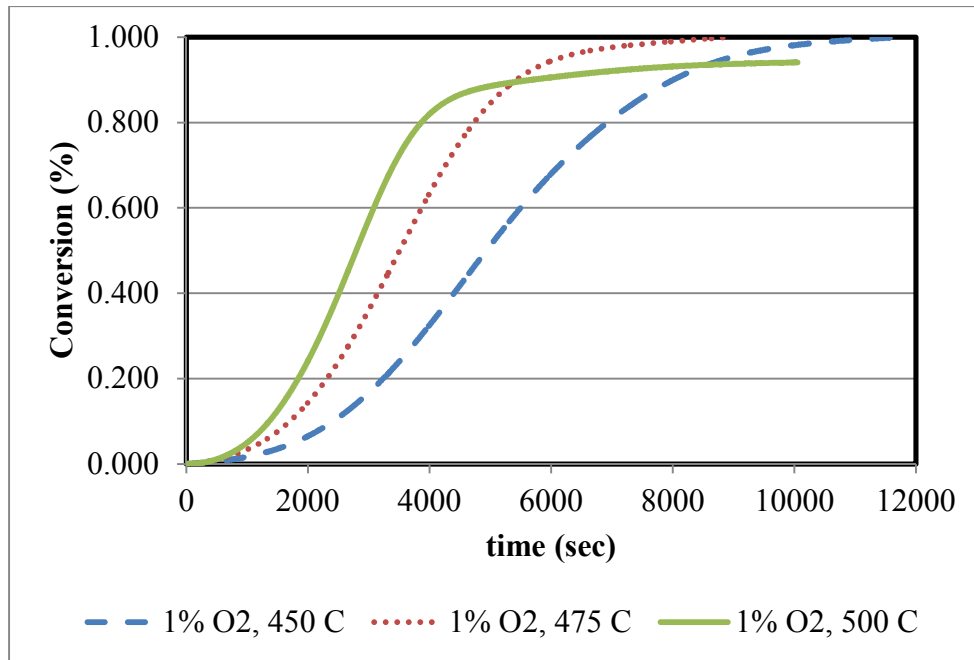


Figure 4-6 - Conversion profiles for asphaltenes chars obtained at 1400°C

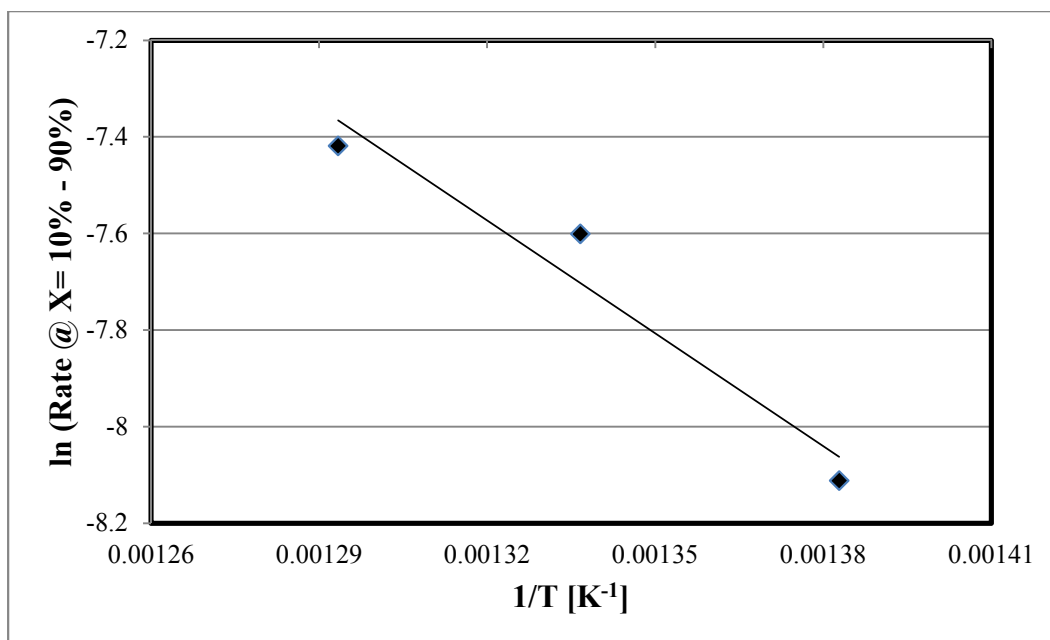


Figure 4-7 - Arhenius plot for asphaltenes char obtained at 1400°C

4.5 Chapter findings and conclusion

The kinetic parameters of asphaltenes and slurry char reaction with O₂ were studied in this chapter. Chars were prepared in an atmospheric drop tube furnace under nitrogen atmosphere at very high temperatures. The validity of the TGA results was discussed and the TGA experiments were carried out in a way that mass transfer diffusion was minimized. The Arhenius plots showed that the experiments were happening in the reaction controlled regime and the effect of mass transfer diffusion was negligible.

Table 4-1 summarizes the kinetic parameters for the asphaltenes and slurry chars.

Table 4-1 - Summary of results for kinetic of char-O₂ reaction

Sample	Pyrolysis temperature °C	Zone I			Zone II		
		E_a	k_0	n	E_a	k_0	n
		kJ/mol	s ⁻¹ Pa ⁻ⁿ	-	kJ/mol	s ⁻¹ Pa ⁻ⁿ	-
Slurry char	1300	99.61	3.04 × 10 ³	0.66	143.28	1.635 × 10 ⁶	0.50
	1400	69.20	10.89	0.58	116.76	14.08 × 10 ³	0.27
Asphaltenes	1400	64.76	15.00	0.45	--	--	--

According to Table 4-1, the activation energy for reaction of coal-asphaltenes slurry char is close to the activation energy of the asphaltene char, both prepared at 1400 °C. This confirms the assumption that in the slurry char, at first the asphaltene part reacts with oxygen and then does the coal part. The differences between other kinetic parameters of slurry and asphaltene char prepared at 1400 °C including k_0 and the order of reaction might be attributed to the effect of mixing coal with asphaltene.

CHAPTER 5

Conclusions and Recommendations

5.1 Conclusions

In this project characteristics of the chars from asphaltenes and Genesee coal-asphaltene slurry that prepared in an atmospheric entrained flow reactor were studied. Chars obtained at high temperature in the range of 800 to 1400 °C. Asphaltene chars prepared at higher temperatures contain more volatile matter, according to the proximate analyses. This is assumed to be happening due to heterogeneous condensation of volatiles on the surface of chars since the chars are cooled down rapidly in the collection

probe. Having more volatiles in larger asphaltenes char particles as well as SEM char images also confirm that assumption. Moreover, TGA reactivity experiments with air showed that pyrolysis temperature does not have significant effect on asphaltenes char reactivity. On the other hand, increasing the pyrolysis residence time decreased the asphaltenes char reactivity and volatile content. Furthermore, the porosity of the char particles was very low.

Moreover, the characteristics of slurry chars obtained at 1200 and 1300°C were close to each other while it was different than 1400 °C one. It can be concluded that pyrolysis temperature higher than 1400 °C has more effect on the char characteristic than the lower pyrolysis temperatures. One of the main findings of this research was comparison between the slurry and asphaltenes chars. It is found that the slurry char reacts with O₂ with two mechanisms since the char is a mixture of coal and asphaltenes. It is found that the reaction with oxygen starts with the asphaltenes part of the slurry char and then it continues with the coal part. Also, it is found that overall reactivity of the slurry char is much lower than the reactivity of the asphaltenes char. Therefore, in terms of the reactivity with oxygen, the mixing of coal with asphaltenes does not have any advantage.

Furthermore, the gasification kinetics of the asphaltenes char and coal-asphaltenes slurry char with oxygen were studied and the kinetic parameters were obtained using isothermal TGA experiments.

5.2 Recommendations for future work

1. The pyrolysis of asphaltenes and coal-asphaltenes was studied at atmospheric pressure in this project. Since most of the industrial reactors operate at higher pressure, this work can be extended to study the pyrolysis at higher pressures.
2. Study of the gasification performance of asphaltenes and slurry feeds in the entrained flow gasifier with different gasifying agents.
3. Extending the kinetic studies of the char reactions with other gasifying agents including CO₂ and steam.

References

- (1) Long, R. B. The concept of asphaltenes. In *Chemistry of Asphaltenes*; ACS: Washington DC, 1981; pp. 17–27.
- (2) *Crude oil forecast, market and pipelines*. Canadian Association of Petroleum Producers, June 2012.
- (3) Higman, C.; Burgt, M. van der *Gasification*; Elsevier: Amsterdam, Boston, 2003.
- (4) Mahinpey, N.; Murugan, P.; Mani, T. Comparative Kinetics and Thermal Behavior: The Study of Crude Oils Derived from Fosterton and Neilburg Fields of Saskatchewan. *Energy & Fuels* **2010**, *24*, 1640–1645.
- (5) Moreno-Arciniegas, L.-S.; Rodríguez-Corredor, F.-E.; Afanador-Rey, L.-E.; Grosso-Vargas, J.-L. Syngas obtainment from the gasification of asphaltenes of the san fernando crude oil. *CT&F - Ciencia, Tecnología y Futuro* **2009**, *3*, 189–202.
- (6) Ashizawa, M.; Hara, S.; Kidoguchi, K.; Inumaru, J. Gasification characteristics of extra-heavy oil in a research-scale gasifier. *Energy* **2005**, *30*, 2194–2205.
- (7) Sirota, E. B.; Lin, M. Y. Physical Behavior of Asphaltenes. **2007**, 2809–2815.
- (8) He, W.; Park, C. S.; Norbeck, J. M. Rheological Study of Comingled Biomass and Coal Slurries with Hydrothermal Pretreatment. *Energy & Fuels* **2009**, *23*, 4763–4767.
- (9) Bekdemir, C. Numerical Modeling of Diesel Spray Formation and Combustion. Master Thesis, Eindhoven University of Technology, 2008.
- (10) Baumgarten, C. *Mixture Formation in Internal Combustion Engines*; Springer: Heidelberg, 2006.
- (11) Cone, H.; Pattern, S.; Cone, F.; Stream, S.; Pattern, F. S. Engineer's guide to spray technology **2000**.
- (12) Clayton T. Crowe *Multiphase flow handbook*; Taylor & Francis: Boca Raton, 2006.

- (13) Buckner, H.N., Sojka, P.E., Lefebvre, A. H. Effervescent atomization of coal-water slurries. *American Society of Mechanical Engineers, Petroleum Division* **1990**, *30*, 105–108.
- (14) Dooher, J. P. . Fundamental considerations for coal slurry atomization. *Atomization and sprays* **2005**, *15*, 585–602.
- (15) Son, S. Y.; Kihm, K. D. Effect of coal particle size on coal-water slurry atomization. *Atomization and sprays* **1998**, 503–519.
- (16) Choi, Y.; Park, T.; Kim, J.; Lee, J.; Hong, J.; Kim, Y. Experimental Studies of 1 Ton / Day Coal Slurry Feed Type Oxygen Blown , Entrained Flow Gasifier. *Korean J. Chem Eng.* **2001**, *18*, 493–498.
- (17) Sakaguchi, M.; Watkinson, a. P.; Ellis, N. Steam Gasification of Bio-Oil and Bio-Oil/Char Slurry in a Fluidized Bed Reactor. *Energy & Fuels* **2010**, *24*, 5181–5189.
- (18) Sakaguchi, M.; Watkinson, a. P.; Ellis, N. Steam gasification reactivity of char from rapid pyrolysis of bio-oil/char slurry. *Fuel* **2010**, *89*, 3078–3084.
- (19) Kolb, T.; Jakobs, T.; Pantouflas, E.; Zarzalis, N. Production of Syngas from Biomass-Based Slurry in an entrained-flow gasifier. In *10th Conference on Energy for a Clean Environment*; 2009.
- (20) Zhang, M.; Chen, H.; Gao, Y.; He, R.; Yang, H.; Wang, X.; Zhang, S. Experimental study on bio-oil pyrolysis/gasification. *Bio resources* **2010**, *5*, 135–146.
- (21) Liu, Y.; Hodek, W.; Van Heek, K. H. Characterization of tar, char and gas from pyrolysis of coal asphaltenes. *Fuel* **1998**, *77*, 1099–1105.
- (22) Zhao, Y.; Wei, F.; Yu, Y. Effects of reaction time and temperature on carbonization in asphaltene pyrolysis. *Journal of Petroleum Science and Engineering* **2010**, *74*, 20–25.
- (23) Fouga, G. G.; De Micco, G.; Bohé, a. E. Kinetic study of Argentinean asphaltite gasification using carbon dioxide as gasifying agent. *Fuel* **2011**, *90*, 674–680.
- (24) Laurendeau, N. M. Heterogeneous kinetics of coal char gasification and combustion. *Prog. Energy Combustt. Sci.* **1978**, *4*, 221–270.
- (25) Murugan, P.; Mahinpey, N.; Mani, T. Thermal cracking and combustion kinetics of asphaltenes derived from Fosterton oil. *Fuel Processing Technology* **2009**, *90*, 1286–1291.

- (26) Latva-Somppi, J.; Moisio, M.; Kauppinen, E. I.; Valmari, T.; Ahonen, P.; Tapper, U.; Keskinen, J. Ash formation during fluidized-bed incineration of paper mill waste sludge. *Journal of Aerosol Science* **1998**, *29*, 461–480.